8-2017

Spatial Mapping and Profiling of Metabolite Distributions During Germination

Adam D. Feenstra
Iowa State University and Ames Laboratory

Liza E. Alexander
Iowa State University and Ames Laboratory

Zhihong Song
Iowa State University

Andrew R. Korte
Iowa State University and Ames Laboratory

Marna D. Yandeau-Nelson
Iowa State University, myn@iastate.edu

See next page for additional authors

Spatial Mapping and Profiling of Metabolite Distributions During Germination

Abstract
Germination is a highly complex process by which seeds begin to develop and establish themselves as viable organisms. In this paper, we utilize a combination of GC-MS, LC-fluorescence, and mass spectrometry imaging (MSI) approaches to profile and visualize the metabolic distributions of germinating seeds from two different inbreds of maize seeds, B73 and Mo17. GC and LC analyses demonstrate that the two inbreds are highly differentiated in their metabolite profiles throughout the course of germination, especially with regard to amino acids, sugar alcohols, and small organic acids. Crude dissection of the seed followed by GC-MS analysis of polar metabolites also revealed that many compounds were highly sequestered among the various seed tissue types. To further localize compounds, matrix-assisted laser desorption/ionization MSI is utilized to visualize compounds in fine detail in their native environments over the course of germination. Most notably, the fatty acyl chain-dependent differential localization of phospholipids and TAGs were observed within the embryo and radicle, showing correlation with the heterogeneous distribution of fatty acids. Other interesting observations include unusual localization of ceramides on the endosperm/scutellum boundary, and subcellular localization of ferulate in the aleurone.

Keywords
amino acids, B73, ceramides, ferulate, germination, maize, mass spectrometry imaging, metabolomics, Mo17, phospholipids

Disciplines
Molecular Biology | Organic Chemistry | Plant Biology | Plant Breeding and Genetics

Comments
This article is published as Feenstra, Adam D., Liza E. Alexander, Zhihong Song, Andrew R. Korte, Marna Yandeau-Nelson, Basil J. Nikolau, and Young-Jin Lee. "Spatial mapping and profiling of metabolite distributions during germination." *Plant Physiology* (2017): 2532. DOI: 10.1104/pp.17.00652 Posted with permission.

Authors
Adam D. Feenstra, Liza E. Alexander, Zhihong Song, Andrew R. Korte, Marna D. Yandeau-Nelson, Basil J. Nikolau, and Young-Jin Lee

Short Title: Metabolite Imaging in Maize Seed Germination

Spatial Mapping and Profiling of Metabolite Distributions During Germination

Adam D. Feenstra[a,b,#] Liza E. Alexander[b,c,d,#], Zhihong Song[d], Andrew R. Korte[a,b], Marna D. Yandeau-Nelson[d,e], Basil J. Nikolau[b,c,d], and Young Jin Lee[a,b,*]

a. Department of Chemistry, Iowa State University, Ames, USA
b. Ames Laboratory-US DOE, Ames, IA, USA
c. Roy J. Carver Department of Biochemistry, Biophysics & Molecular Biology, Iowa State University, Ames, IA, USA
d. Center for Metabolic Biology, Iowa State University, Ames, IA 50011
e. Department of Genetics, Development & Cell Biology, Iowa State University, Ames, IA, USA
#. These authors equally contributed.
*. Correspondence: Young Jin Lee, 35A Roy J. Carver co-Lab, Department of Chemistry, Iowa State University, Ames, IA 50010. E-mail: yjlee@iastate.edu

One Sentence Summary: A combination of metabolomics and mass spectrometry imaging provides new insights in metabolic processes during the germination of maize seeds.

Y.J.L. conceived the idea; A.D.F., M.D.Y-N., B.J.N. and Y.J.L. designed the experiments; B.J.N. and Y.J.L. supervised experiments; A.D.F. and L.E.A. performed most of the experiments and data analysis; Z.S. and A.R.K. performed some experiments and data analysis; A.D.F., L.E.A., M.D.Y-N., B.J.N. and Y.J.L. wrote the manuscript.

This work was supported by the US Department of Energy (DOE), Office of Basic Energy Sciences, Division of Chemical Sciences, Geosciences, and Biosciences. The Ames Laboratory is operated by Iowa State University under DOE contract DE-AC02-07CH11358.

*Address correspondence to yjlee@iastate.edu.

Abstract

Germination is a highly complex process by which seeds begin to develop and establish themselves as viable organisms. In this paper, we utilize a combination of GC-MS, LC-fluorescence, and mass spectrometry imaging (MSI) approaches to profile and visualize the metabolic distributions of germinating seeds from two different inbreds of maize seeds, B73 and Mo17. GC and LC analyses demonstrate that the two inbreds are highly differentiated in their metabolite profiles throughout the course of germination, especially with regard to amino acids, sugar alcohols, and small organic acids. Crude dissection of the seed followed by GC-MS analysis of polar metabolites also revealed that many compounds were highly sequestered among the various seed tissue types. To further localize compounds, matrix-assisted laser desorption/ionization MSI is utilized to visualize compounds in fine detail in their native environments over the course of germination. Most notably, the fatty acyl chain-dependent differential localization of phospholipids and TAGs were observed within the embryo and radicle, showing correlation with the heterogeneous distribution of fatty acids. Other interesting observations include unusual localization of ceramides on the endosperm/scutellum boundary, and subcellular localization of ferulate in the aleurone.

Key Words: amino acids, B73, ceramides, ferulate, germination, maize, mass spectrometry imaging, metabolomics, Mo17, phospholipids

INTRODUCTION

Plants use seeds as the propagule to ensure reproduction to the next generation, and over the past 10,000 years human civilizations have established agricultural practices to ensure a seed-based food supply (Larson et al., 2014). Therefore, deciphering the processes that enable seeds to perform their biological functions is of importance in understanding how plants are propagated, and is also of practical importance to improve agriculture. Seeds are designed to survive long periods of dormancy in a relatively dry state, and the process of germination is initiated by the imbibition of water. During this germination process, many metabolic changes occur, most of which are associated with the catabolism of seed storage products (proteins, polysaccharides and lipids) into metabolically useable, simpler chemical forms that are either used as precursors to assemble the growing seedling or are oxidized via energy-producing biochemical pathways to thermodynamically support growth (Bewley, 1997, 2001).

The specific metabolic processes that support seed germination are somewhat dependent on the taxonomic clade of the plant, which determines seed tissue/organ organization and the nature of the seed storage compounds. Specifically, the seeds of the Poaceae family of monocots are characterized by a starch- and protein-filled endosperm, and their catabolism by digestive enzymes produced in the outermost layer of the endosperm (i.e. the aleurone) provides the carbon-based and nitrogenous precursors for the growth of the embryo, which is comprised of the embryonic axis and the scutellum (Dante et al., 2015). Thus, during seed germination the glycolytic and oxidative pentose phosphate pathways are induced to metabolize the hydrolyzed starch. The smaller quantities of seed storage proteins are also catabolized to provide the amino acid precursors for new protein synthesis in the embryo, or carbon-skeletons for re-assimilation into anabolic processes or further catabolized for energy generation. Finally, lipid in the form of triacylglycerol is stored in a specialized tissue (in maize, the scutellum), and its catabolism via the beta-oxidation of fatty acids can provide the elongating embryo axis an energy source. Alternatively, coupling with the glyoxylate pathway, which is induced during germination, carbon from fatty acids can be used to assemble new metabolic intermediates to support embryo-growth (Firenzuoli et al., 1968; He et al., 2015).

Thus, seed germination requires the coordinated induction of a number of processes that are non-uniformly distributed among the tissues and organs of the seed. Many of the metabolic

pathways that are induced during the seed germination processes that involve starch, oil, and protein turnover have been studied via molecular, genetic, and biochemical studies (Ingle et al., 1964; Limami et al., 2002; Shu et al., 2008; Zhang et al., 2009). Therefore, techniques that allow for the determination of spatial localization of metabolites in fine detail, specifically mass spectrometry imaging (MSI), should allow for further insight into the mechanisms and actions of the pathways that are integral to seed germination.

MSI has become an increasingly powerful technique to provide spatial distribution of biological molecules within tissues (McDonnell and Heeren, 2007). In a typical MSI experiment, a sampling probe is rastered across a tissue sample with mass spectra collected at each raster point. Following data acquisition, the spatial distribution of ions of interest can be visualized based on the x-y coordinates of the collected spectra. Various sampling probes have been adopted for MSI along with accompanying ionization methods (McDonnell and Heeren, 2007; van Hove et al., 2010). Owing to its ease of use, high sensitivity, and ability to ionize a wide variety of molecules, matrix-assisted laser desorption/ionization (MALDI) has been the most widely used MSI technique. MALDI-MSI can obtain high-spatial resolution images of ions, allowing for visualization of fine structures. Spatial resolution of ~20 μm size has become routine in MALDI-MSI, and 2-5 μm spatial resolution has been demonstrated by several groups, with the latter providing a means for locating metabolites within subcellular compartments (Zavalin et al., 2013; Korte et al., 2015).

Recently, MALDI-MSI has begun to see increased application in the study of plant biology (see recent comprehensive reviews, (Kaspar et al., 2011; Lee et al., 2012)). Here, we applied MALDI-MSI in combination with GC-MS and HPLC-based analyses of extracts to study the distributions and profiles of metabolites in germinating maize seeds at four different time points after imbibition. Two contrasting maize genotypes (inbreds B73 and Mo17) were compared during germination to explore the metabolic differences arising from the genetic differences between these two inbreds. GC-MS and HPLC-based metabolite profiling of extracts prepared from the physically dissected seeds was used to distinguish between the metabolomes of the two inbreds during early germination, and provide a quantitative validation of the MSI localization data. Three different MALDI matrices were used in either positive or negative ion mode to image the spatial distribution of a wide range of metabolites. This integrated approach provides unprecedented insights into the spatially resolved coordination of metabolic processes

that are sequestered among the germinating embryo axis, the lipid rich scutellum, the nutritive endosperm, the digestive aleurone, and outer pericarp cell layers during the early stages of seed germination.

RESULTS

Overview of Experimental Workflow

A schematic of the experimental workflow is provided in Fig. 1. Maize seeds were collected from the B73 and Mo17 inbreds at four time points during the early phases of germination (0.2-h, 12-h, 24-h and 36-h post imbibition). At each time point, 9 seeds comprising three biological replicates (3 seeds each) were immediately flash frozen and extracted for whole-seed metabolite profiling. These extracts were analyzed via a GC-MS non-targeted global metabolite analysis platform, and via an LC-fluorescence based targeted analysis platform for amino acids. In addition, at the 12-h and 36-h time points, 9 seeds comprising three biological replicates (3 seeds each) were collected for GC-MS analysis of seeds dissected into component endosperm, embryo, tip-cap and pericarp. In parallel, 3 additional seeds from each of the four time points were flash frozen in liquid nitrogen and were subjected to MSI analysis. These seeds were sectioned with 10 μm thickness (25 sections per seed) and four sections (#s 5, 11, 17, 22) were inspected via optical microscopy. The three sections nearest to the most intact section as determined via optical microscopic inspection were used for MSI analysis. Microscopic analysis revealed detailed morphological features of the seed that include: the pericarp, which is the outermost layer of the seed, the aleurone layer of the endosperm, the endosperm itself, the embryonic axis, the scutellum and the tip-cap. As germination progressed, the radicle also became visible as it protruded from the embryonic axis of the embryo. It is important to note that it can be difficult to distinguish between the multicellular pericarp and the single cell aleurone layer at lower magnification. In the cases where these cell layers cannot be distinguished, we will refer to these as the aleurone and/or pericarp.

The analytes that can be characterized through MSI are often significantly limited by the choice of matrix and ion polarity. In this work, MSI analysis was performed on the three tissue sections with one of three different matrices, 1,5-diaminonaphthalene (DAN), 9-aminoacridine (9AA), and 2,5-dihyroxybenzoic acid (DHB), to cover a relatively wide range of analytes. DAN and 9AA were used in negative ion mode (*m/z* range 50-1000), while DHB was used in positive

ion mode (*m/z* range 50-800, and *m/z* range 600-1600). In total, 72 seed sections were analyzed by MSI (2 inbred lines x 3 seeds per time point x 4 time points x 3 sections per seed for each of the three matrices). A spatial resolution of 100 μm was used to minimize the total data acquisition time in this large-scale experiment, while still providing sufficient spatial resolution to match the morphological features observed in the optical images.

Over the course of the analyses, hundreds of analytes were observed by both MSI and the GC- and LC-based metabolite profiling platforms. However, due to biological and analytical variation, many low abundance analytes were not reproducibly detected across all data sets. We therefore limit our discussion to the more abundant analytes that were consistently observed across three biological replicates. For simplicity of presentation of the MSI data, all the *m/z* values and mass tolerances used in producing images are summarized in Table S1, as well as color scales used to produce false color images.

Analysis of the metabolomes of germinating seeds

The non-targeted GC-MS metabolomics analyses of the whole seeds at four germination time points detected 162 analytes, of which 63 were chemically identified. These metabolites include sugars (monosaccharides and disaccharides), sugar acids, organic acids, phenolics, nitrogenous metabolites, polyols, esters, lipids, fatty acids and sterols (Table S2). There are clear differences in the metabolome between the two inbreds, and the metabolite profile is also affected by the germination process. Using the log-ratio plots, we evaluated the degree to which these differential metabolites between the inbreds are differentially affected by the germination process (Fig. 2A). In these comparisons we used the 12-hour time point as the "anchor" for all comparisons among genotypes and the seed germination time line. At this anchor time point, there are 63 metabolites that accumulate at significantly different levels between the inbreds. By comparing such log-ratio data at each of the four time points, one can gain insights of how the germination process affects the metabolome. One readily recognizable class of metabolites that are clearly distinct between the two inbreds is the amino acids, and this platform detected 10 of the proteinogenic amino acids. We therefore confirmed these differences with a second analytical platform, which specifically targeted amine-containing metabolites with LC-fluorescence, and this detected 18 of the proteinogenic amino acids (Table S3), the exceptions being proline and cysteine. In both the targeted LC-amino acid platform (log-ratio plot in Fig.

S1) and the non-targeted GC-MS metabolomics platform (Fig. 2A), most amino acids are at significantly higher levels in Mo17 seeds than B73. These data are consistent with previous studies of these inbreds that identified Mo17 mature seeds having a higher amino acid content than B73 (Römisch-Margl et al., 2010). As the germination process proceeds, these differences in amino acid content between the two inbreds is reduced, so that by 36-h post-imbibition the profiles are almost identical except for Lys, Thr, and Arg that are still slightly higher in Mo17 and Trp that is now slightly higher in B73 (Fig. S1).

More broadly, 64% of the detected metabolome (i.e., 104 metabolites) accumulates to different levels between the two inbreds at least at one time-point during the germination process ($p<0.05$ in Table S2). Among the 104 metabolites that accumulate differentially among any of the time-points, 21 are differential at all time-points evaluated (Fig. 2B), and 15 are differential among any of three consecutive time-points. Seven of the first group are chemically identified and appear to be intermediates of metabolic processes that would be expected to be hyperactive during seed germination. These are specifically associated with carbohydrate metabolism (i.e., sorbitol, cellobiose, rhamnose and talose), which may be associated with starch mobilization that is occurring during the breakdown of the endosperm tissue, or possibly cell wall deposition as the new seedling tissues begin to be assembled. Eight of the chemically identified metabolites that are differential among the 3 consecutive time-points are amino acids (i.e., Asp, Glu, Thr) in the 3-early time points, and lipids (i.e., stigmasterol, sitosterol and linoleic acid) that are differential among the 3 latter time points. These profiles are consistent with seed storage protein mobilization, which occurs at the earlier stages of seed germination, and membrane deposition occurring later in the process as the seed radicle begins to grow and emerge. Finally, among these chemically identified differentially expressed metabolites are succinic acid and fumaric acid, which as intermediates of the TCA cycle and these would be associated with high rates of respiration that is needed to support the germination process (Bewley *et al.*, 2012). Collectively these data indicate that these metabolic processes are differential between the two inbreds, which correlates with the phenotypic observation that these two inbreds germinate at different rates.

Bearing in mind that a germinating maize seed consists of different tissues, each of which express diverse metabolic processes, we evaluated the distribution of the metabolome among four distinct seed organs that are readily separable by microdissection (i.e., the pericarp and

aleurone layers, the embryo, endosperm and tip-cap). The metabolomes of these microdissected organs were evaluated at 12-h and 36-h post-imbibition. Because of the wider range of metabolites that were detected, the GC-MS analysis of the metabolomes of the microdissected seed organs focused on the polar class of metabolites. These analyses revealed the relative abundances of 218 analytes, of which 75 were chemically defined (Table S4). Fig. S2 shows the log-ratio plot for the relative abundances of all analytes between Mo17 and B73, comparing the metabolomes of each dissected organ and the metabolomes of the whole seed.

An obvious advantage in the micro-dissected dataset is that it reaches lower abundance metabolites, revealing the relative abundances of an extra 56 analytes (Table S4) that were not detected when whole seeds were analyzed. More significantly, the metabolites that are the most differential between the metabolomes of the whole seed are different when one considers the metabolomes of the separated organs, which is indicative of the different metabolic processes that are being expressed in these individual organs. At both time-points, the endosperm and embryo tissues account for the majority of the differentially expressed metabolites. About half of these are shared among multiple evaluated organs, but about 20% of the metabolome is uniquely differential in either the embryo or endosperm tissues (Fig. 2C and 2D). The endosperm specific differential metabolites are primarily amino acids at 12-h post-imbibition, but by 36-h these are a mixture of amino acids, sugars and organic acids. This is consistent with the degradation of the starch and seed storage proteins that are concentrated in the endosperm of maize seeds, and indicate different rates of their catabolism between the two inbreds.

Therefore, these data indicate that as the seed germination process proceeds, the expressed metabolome changes between inbred lines with larger changes occurring in the embryo, followed by the endosperm and tip-cap. Fewer differentially expressed metabolites occur in the metabolome of the pericarp and aleurone tissues. More refined analyses of the non-uniform distribution of the metabolites in the different tissues of the germinating maize seed was obtained by MS-imaging.

Heterogeneous distribution of the mobilization of seed storage reserves

In the grasses, energy in dormant seeds is predominantly stored as polysaccharide starch granules within the endosperm, which can be mobilized by hydrolytic enzymes (e.g. α- and β-amylases) released by the aleurone and scutellum of germinating seeds (Zeeman et al., 2007).

The images in Figure 3A show large hexose polysaccharides (Hex_{5-9}), presumably degraded from starch, are observed at low abundance levels and are localized in the endosperm. Disaccharides, predominantly sucrose, are also observed and are present at much higher levels and primarily constrained to the germinating embryo. At the later stages of germination, the disaccharide signal appears to be concentrated more extensively in the emerging radicle of the embryonic axis. Disaccharide is also detected within other tissues such as the endosperm and pericarp and/or aleurone, but at lower abundance. These non-homogeneous distributions of the polysaccharides are conserved in both B73 and Mo17 inbreds, and are consistent with the mobilization of sucrose within the scutellum and transport to the embryonic axis, specifically the radicle (Sánchez-Linares et al., 2012).

Seed oil energy reserves in maize are localized to the embryo, which is in contrast to other cereal grains (e.g. wheat and oat) that store oil in the endosperm (Leonova et al., 2010). Embryonic localization of four TAG species differing in fatty acyl chain composition is shown in Fig. 3B. At the initial stages of germination (i.e. 0.2 and 12-h), TAGs are homogeneously distributed throughout the embryo, including the embryonic axis and the scutellum. As germination progresses and the radicle of the embryonic axis begins to elongate, TAGs begin to display non-uniform localization patterns, similar to fatty acid and phospholipid molecular species, as will be discussed later.

During the germination process, amino acids become available from the breakdown of storage proteins initiated by the hydrolytic activity of protease enzymes synthesized in the protein storage vacuoles (PSV). The reduced nitrogen associated with these amino acids can be used for additional *de novo* synthesis of amino acids (Bewley et al., 2012). Because of their low ionization efficiency and amphiprotic nature, amino acids are difficult to analyze by MALDI-MS (Toue et al., 2014). Despite this known difficulty, three amino acids were reliably detected in the MSI experiments, these being lysine, arginine, and proline (Fig. 3C). Lysine and arginine are barely detectable in B73 seeds, but are clearly visible in Mo17 seeds. This striking difference in the abundance of lysine and arginine between the two inbreds is consistent with the parallel profiling data of these amino acids generated by LC-fluorescence analysis of o-phthaldialdehyde (OPA)-derivatives conducted on extracts of seeds (Fig. S1); the concentrations of these amino acids are significantly lower in extracts of B73 seeds than Mo17 seeds throughout the germination process. The LC method could not analyze proline levels in these extracts because

the OPA-derivatization requires a primary amine group. Rather, proline concentrations were compared from parallel GC-MS analyses of the polar extracts of seeds (Fig. 2A and S2). These data are in agreement with the MALDI-MSI data, with proline levels being similar or slightly higher in B73 seeds than Mo17 seeds. The MSI-data establish that the accumulation of these amino acids (lysine, arginine and proline) is concentrated in the embryonic axis and the scutellum of the seed embryo. Moreover, in later time-points, proline is more prominent in the radicle of the seed, but lysine and arginine appear to be less abundant in the radicle. These MSI-based visualizations of the *in situ* localization of these amino acids are consistent with the direct quantitative measurement of the levels of these amino acids in extracts of micro-dissected embryo tissues of the maize seeds (Fig. S3).

Metabolites enriched in pericarp/aleurone layers

The pericarp and aleurone layers of the seed are responsible for the protection of the mature seed, as well as the initial uptake of water that begins germination. As germination begins in maize, many of the enzymes needed to break down storage molecules in the seed are released from the aleurone layer of the endosperm (Chrispeels and Varner, 1967; Fincher, 1989; Bernier and Ballance, 1993). In this work, three metabolites are found to be uniquely located at the perimeter of the cross-section and therefore can be surmised to be located either in the pericarp (outermost layer of the kernel) or the aleurone layer, which is the outermost single-cell layer of the endosperm. The three metabolites remained localized to this region of the seed throughout the germination process, and were not detected in the embryo or the endosperm (Fig. 4A). This is in contrast to most other metabolites, such as sucrose (Fig. 3A) or citrate (Fig. 5), that are found in the aleurone and/or pericarp, but also in other tissues. One of these metabolites (*m/z* 193.051) was identified as ferulate by accurate mass (< 5ppm) and MS/MS (Fig. S4). However, useful MS/MS spectra could not be obtained for the other two ions (*m/z* 135.046 and *m/z* 161.025) because of their low abundance. The chemical compositions calculated from the accurate masses, $C_8H_8O_2$ and $C_9H_6O_3$, respectively, suggest they may have at least one aromatic ring.

The spatial resolution used in this experiment, 100 μm, was not sufficient to determine whether these metabolites are specifically localized to the multiple cell layers of the pericarp or the single-cell layer of the aleurone. To further explore the exact location of these compounds, a high-resolution MSI experiment was performed with 10 μm spatial resolution on a small region

of the outer perimeter of B73 maize seeds at 24-h post-imbibition (Fig. 4B, 4C). Because of the limited sensitivity inherent with a much smaller sampling area, only ferulate provided sufficient ion signal to produce a clear image. The ferulate image was compared with that of the phospholipid phosphatidylinositol (PI) 34:2 and malate to better understand the relative localization of these compounds. Comparing these molecular images with the corresponding optical image (Fig. 4B) and overlaying MS images with the optical image (Fig. 4C), ferulate (red) appears to be present exclusively in the aleurone layer, particularly at the boundary between the aluerone and the pericarp, while the phospholipid PI 34:2 (green) is present throughout the aleurone layer, and malate (blue) is localized in the endosperm and the pericarp layer of the seeds.

Localizations of Respiratory Intermediates - Phosphorylated Metabolites and Organic Acids

During the process of seed germination, respiration of seed reserves enables energy generation in the absence of photosynthesis, supporting the development of the seedling until it protrudes from the soil and is able to harness solar energy via photosynthesis. Respiration initiates within minutes of imbibition by the activation of cytosolic enzymes for glycolysis, the oxidative pentose phosphate pathway, and enzymes for the TCA cycle in mitochondria (Bewley et al., 2012). The distributions of two phosphorylated intermediates of respiration, hexose phosphate and glycerol phosphate, and one or possibly two organic acids of the TCA cycle, citrate and/or isocitrate, are shown in Fig. 5. The phosphorylated metabolites are most likely glucose-6-phosphate and glycerol-3-phosphate, respectively, but we cannot distinguish among the possible regio- or stereoisomers by MALDI-MS or MS/MS experiments. Similarly, we are also unable to distinguish between citrate and isocitrate, and the resulting image is likely an integration of the distribution of these two metabolites.

In both inbreds, hexose phosphate and glycerol phosphate are localized in the germinating embryo and the aleurone and/or pericarp of the seeds, and this location is unaltered throughout the germination process. Hexose phosphate appears to be slightly less abundant in the radicle, whereas glycerol phosphate is more homogeneously distributed throughout the embyro. The organic acids, citrate/isocitrate, are observed first at 0.2-h post-imbibition, and they are predominantly concentrated in the perimeter (i.e. the aluerone and/or pericarp) of the seed. As germination progresses, citrate/isocitrate also occurs within the radicles and scutella of both

inbreds, similar to the hexose phosphate and glycerol phosphate compounds; the former is probably associated with the induction of the glyoxylate pathway or TCA cycle, which is induced during germination to convert lipid-derived carbon to sugars via acetyl-CoA intermediate, while the latter two are an intermediate and side product of glycolysis, respectively (Bewley et al., 2012).

Malate is another molecule involved in the TCA cycle and is detected in all replicates at all time points. Unlike citrate, its localization is found only in the endosperm of the seed and radicle of some more fully developed seeds (Fig. S5A). This is not compatible with GC-MS analysis of the micro-dissected seed samples that indicated most of the malic acid is present in the embryo of the seed rather than the endosperm (Fig. S5C). In contrast, citrate is much more abundant in embryos (Fig. 5) matching well with the dissected GC-MS data (Fig. S5D). According to our previous experience on MSI of leaf tissues, malate is often difficult to obtain reproducible results unless the tissues are prepared fresh and analyzed as soon as possible. Hence, we suspect this observation may be an artifact coming from the degradation of malate during tissue storage. To confirm this hypothesis, a separate MSI experiment was conducted on a seed that was analyzed on the same day it was collected. In this experiment, we found the majority of the malic acid in the embryo as expected (Fig. S5B).

Differential distributions of lipid classes accentuated in the emerging radicle

In monocotyledons (i.e. monocots) such as maize, the embryonic axis develops into two main parts: the radicle, which is the primary root and is protected by the coleorhiza, and the plumule, or collection of leaf primordial, which is protected by the coleoptile. The germination process transitions into seedling growth with the protrusion of the radicle from the embryo. These anatomical structures develop with significant cell extension with or without cell division. Radicle growth through cell extension is a turgor-driven process that will involve the assembly of new membranes, requiring lipid biosynthesis (Bewley, 1997, 2001). We therefore applied MALDI-MSI to localize lipids during the germination process. MALDI-MS efficiencies are dramatically different for each lipid class, depending on their chemical functionalities. Three matrices were used in positive and negative ion modes to visualize different classes of lipids. DHB was used in positive ion mode for phosphatidylcholine (PC) and ceramides; 9AA was used

in negative ion mode for fatty acids; and DAN was used in negative ion mode for phosphatidylethanolamine (PE), phosphatidic acid (PA) and phosphatidylinositol (PI).

Fig. 6 compares the spatial distribution of four fatty acids, palmitate (16:0), stearate (18:0), oleate (18:1), and linoleate (18:2) between the two inbreds at four germination stages. Over the course of the germination process, palmitate and linoleate occur homogeneously throughout the embryo in both inbreds. In contrast, stearate is partially and oleate is almost completely absent from the radicles of both inbreds. This unprecedented finding is similar to the localization of TAGs (Fig. 3), and phospholipid classes (Fig. 7). However, it is in contrast to the GC-MS metabolomics data, which do not provide any spatial localization information for these fatty acids between the genotypes or changes associated with germination time points (Fig. S6), and do not offer any indication of this unique, non-uniform localization of oleate.

The spatial localization of four different classes of phospholipids (PE, PA, PI and PC) was compared in germinating seeds at 36-h post-imbibition (Fig. 7A). These analyses also evaluated the distribution of different phospholipid molecular species arising from different combinations of fatty acyl chains. As may be expected from the fact that new cells are being generated as the embryo is undergoing expansion (in contrast to the endosperm, which is being consumed), all four phospholipids are most highly abundant in the embryo. There are contrasting localization patterns depending on the phospholipid class and on the molecular species of the phospholipids. With all four phospholipids and in both inbreds, the phospholipids with the most unsaturated acyl chains (36:4) show an even distribution between the radicle and the other embryonic tissues. For PI, PC, and PA, the more saturated phospholipids (i.e., in the order of 36:3, 36:2, and 36:1) are less concentrated in the radicle as compared to other embryonic tissues. In contrast, PE shows a unique localization pattern, with molecules of an even number of double bonds (36:4, 36:2) being homogeneously distributed over the entire embryo, including the radicle, but PEs with an odd-number of double bonds (36:3, 36:1) being less abundant in the developing radicle. These differential localization patterns were also observed at all time points during the germination process (Fig. S7).

To further investigate the non-uniform distribution of phospholipids, quantitative comparison was made from two mass spectra averaged over selected pixels from the radicle and scutellum of seeds developed with a radicle. Fig. 7B shows the ratio of each lipid molecular species, comparing signal strength for pixels in the radicle to the signal strength for pixels in the

388 scutellum. This analysis confirms the visual patterns observed from the MS images; namely, the
389 signal strength for the more saturated PA, PI, and PC is lower in the radicle region, whereas the
390 signal strength of PE is lower only for those species with an odd number of double-bonds. The
391 unique localization of PE compared to the other phospholipid molecular species may be related
392 to the unusually high abundance of PE 36:2. Fig. 7C illustrates these abundance differences
393 among the phospholipids in the radicle region. Whereas the most abundant molecular species
394 are 36:4 for PC, PA and PI and the more saturated forms of these phospholipids occur at lower
395 levels, 36:2 is the most abundant PE, followed by PE 36:4. With the exception of PE 36:2, which
396 is slightly, but statistically higher in Mo17 than in B73 ($p\sim0.01$) and accordingly lower
397 abundance of PE 36:4 ($p\sim0.03$), there are no other significant differences between the genotypes.
398 The differential localization of phospholipids between the radicle and scutellum of the
399 embryo is consistent with the relatively lower abundance of oleate (18:1) in the radicle (Fig. 6).
400 To investigate this possible correlation, we took advantage of the MS/MS capabilities of the
401 MALDI-MS instrument used in this study and performed MS/MS imaging experiments. In
402 MS/MS, a specific precursor ion can be selected and fragmented, and the mass spectra of
403 fragment ions can be interpreted to extract structural information of the precursor ions. In the
404 current MS/MS imaging experiment, a four-step data acquisition pattern (Fig. S8) was used to
405 selectively acquire the MS/MS data for four PA and PE molecular species (PE 36:3, PE 36:2, PA
406 36:3 and PA 36:2). Fig. 8A shows MS/MS spectra obtained from the MS/MS imaging
407 experiment for PA 36:2 and PE 36:2 in the radicle region of a 24-hr Mo17 seed (similar results
408 were seen for B73). For these 36:2 lipid species, there are two fatty acyl chain combinations
409 possible: 18:2/18:0 and 18:1/18:1. The MS/MS spectrum of PA 36:2 has each of the three fatty
410 acyl fragments (18:2, 18:1, and 18:0), indicating the presence of both the 18:2/18:0 and
411 18:1/18:1 combinations. In contrast, MS/MS of PE 36:2 shows only the 18:2 acyl fragment in the
412 radicle of Mo17, indicating it is primarily comprised of the 18:2/18:0 combination. Because
413 MS/MS preferentially induces fragmentation at the sn-2 position for PE and PA species (Hou et
414 al., 2011), the inability to observe the 18:0 acyl fragment could indicate that PE 36:2 has the 18:2
415 fatty acyl chain predominantly located at the sn-2 position. Parallel MS/MS experiments of PA
416 36:3 and PE 36:3 reveals the occurrence of both 18:2 and 18:1 acyl fragments, confirming the
417 occurrence of these two fatty acyl chains in these lipids (Fig. S9).

Relative quantification between 18:2/18:0 and 18:1/18:1 was performed from this dataset for PA and PE species in the radicle and scutellum, as shown in Fig. 8B. Similar to Fig. 7B and 7C, in this calculation MS/MS spectra were averaged from pixels in the radicle and the scutellum, and fatty acyl fragments were summed to calculate the proportion of each molecular species. It should be noted, however, that because of the difference in the fragmentation efficiency between sn-2 and sn-1 positions this is not an exact quantification of the four lipids. Regardless, these calculations indicate that PE 36:2 (18:2/18:0) is the predominant PE species both in the radicle and scutellum, matching the homogeneous images of the distribution of PE 36:2 (Fig. 7A), and of linoleate (Fig. 6) throughout the embryo. In contrast, PA 36:2 (18:1/18:1) occurs at significantly higher levels in the scutellum than in the radicle, consistent with the heterogeneous distribution of oleate among these two tissue types (Fig. 6).

The non-symmetric distribution of 18:2-containing phospholipids between scutellar and radicle tissues suggests that the supply of 18:2-fatty acid maybe differential between these two tissues. We directly tested this hypothesis by assaying the expression of the fatty acid desaturase that converts 18:1 to 18:2. Specifically, we evaluated *FAD2* mRNA levels by qRT-PCR using RNA isolated from the dissected scutellar and radicle tissues. Bioinformatic analysis of maize genome data (Sen et al., 2010; Petryszak et al., 2016) identified six putative *FAD2* genes based upon sequence homology to the Arabidopsis *FAD2* gene (At3g12120); these being annotated as GRMZM2G169240, GRMZM2G169261, GRMZM2G174766, GRMZM2G056252, GRMZM2G161792 and GRMZM2G064701. Initial assays (Table S5) identified that only GRMZM2G056252 and GRMZM2G064701 are expressed at measurable levels in germinating embryonic tissue during the initial 36-hours after imbibition; the expression of the other 4 FAD2-like genes were detectable by RT-PCR, but their levels were too low to obtain robust quantitative expression data. However, later in the germination process (at 48 hours post-imbibition), 2 of these *FAD2*-like genes were induced (i.e., GRMZM2G169240 and GRMZM2G169261) (Table S5), but this induction was not relevant to testing of the MSI-generated hypothesis.

Fig. 9 shows the expression profile of the GRMZM2G056252 and GRMZM2G064701 mRNAs over the seed germination time-period evaluated by MSI and metabolomics analyses. These data indicate that these two *FAD2* genes are initially expressed at similar levels between the radicle and scutellar, but expression subsequently increases in the radicle by between 3- to 7-fold. This increased expression in the radicle occurs in both inbreds (B73 and Mo17), reaching

449 peak expression at 36-hours post-imbibition. These data are consistent with the elevated levels of
450 18:2-containing PE in the radicle.

451 Several ceramide (Cer) molecular species were also observed in both inbreds, and their
452 accumulation is persistent throughout the course of germination. Fig. 10A shows the distribution
453 of Cer d42:1 and Cer t42:0, and the distributions of other Cer species (Cer d42:2, d40:1, t40:0)
454 are shown in Fig. S10. We have previously performed MS/MS of Cer d42:1 in germinated B73
455 maize seed confirming its structure (Feenstra et al., 2015), and we are also confident of the
456 assignment of other ceramides based on the accurate mass determinations of the ions, all within 5
457 ppm mass error; however, MS/MS was not successful for other ceramides due to their low
458 abundances. All ceramides have unique localization patterns that are different from the other
459 lipid classes that were imaged. In both inbreds, and throughout the course of germination, all the
460 detected ceramides are located on the endosperm side of the endosperm-scutellum boundary. Fig.
461 10B shows this contrasting localization, comparing the distribution of Cer d42:1 with the
462 embryo-specific PC 34:2, relative to the endosperm-scutellum boundary.
463

464 **Discussion**

465 The process of seed germination is a particularly interesting biological process driven by
466 cellular and metabolic coordination among several spatially distinct compartments to
467 successfully establish the seedling. Because of the agricultural importance of cereal grains,
468 previous metabolomics-based work has focused on these processes during the germination of
469 rice (Shu et al., 2008) and the malting process for barley (Frank et al., 2011). However,
470 traditional metabolomics analyses often prove laborious and challenging, with limited spatial
471 information. Conversely, MSI presents a straightforward analytical capability that provides high-
472 resolution spatial distribution data for small metabolites (< 1.5 kDa) but at the cost of limited
473 quantitative information and total number of metabolites detected. In this work, a combination of
474 GC- and LC-based metabolomics analyses were combined with an MALDI-MSI approach to
475 study the quantitative metabolite profile data and spatial distribution of metabolites during the
476 germination of seeds of two maize inbreds, Mo17 and B73. These complementary strategies
477 provided a path to investigate both genotypic and developmental differences that occur during
478 germination, as well as provide quantitative and finely-detailed spatial localization of
479 metabolites.

480 The genetic diversity within maize is vast, as recently evidenced by rampant structural
481 variation in genic content and copy number variation across maize inbreds (Springer et al., 2009;
482 Lai et al., 2010; Swanson-Wagner et al., 2010; Hirsch et al., 2014). Inbreds B73 and Mo17 were
483 selected in state-sponsored public breeding programs led by Land Grant institutions Iowa State
484 University and University of Missouri, respectively in the early 1900s continuing to today. B73
485 is derived from the Stiff Stalk Synthetic population generated and maintained at Iowa State
486 University and Mo17 was selected from Lancaster Sure Crop material first developed in
487 Lancaster, PA (Troyer, 2004). The B73 and Mo17 inbreds share a rich history in the public
488 sector as key founders of U.S. germplasm (Lu and Bernardo, 2001) and development of
489 agronomically important hybrids, both in the public and private sectors (Troyer, 2009). These
490 important inbreds differ significantly in their genomic structures, both in terms of presence-
491 absence variation in gene content as well as in the prevalence of single nucleotide
492 polymorphisms, occurring on average every ~80 bp (Fu et al., 2006; Vroh Bi et al., 2006) based
493 on comparison of published genome sequence (Schnable et al., 2009). The genetic diversity
494 between B73 and Mo17 translates into metabolic, physiological and phenotypic differences,
495 including differences in germination rates and germination efficiency for inbreds B73 and Mo17
496 that have been observed under different environmental conditions (Munamava et al., 2004). This
497 genetic diversity between the two inbreds has also led to differences in the metabolome, as was
498 observed in our metabolic assessment of early germination of maize seedlings. The most
499 significant metabolic difference between germinating B73 and Mo17 seeds was in the enhanced
500 accumulation of free amino acids in Mo17.
501 The fact that four of the amino acids (i.e. Arg, Asn, Gln, Lys) showing higher abundance
502 in Mo17 vs. B73 are the carriers of reduced nitrogen may indicate that these metabolic processes
503 are of significance in the interaction between carbon and nitrogen metabolism, as the
504 germinating seeds adjust the physiological needs of the emerging seedling from different starting
505 points in the amino acid profiles available in each inbred. Consistent with this hypothesis is the
506 fact that these amino acid profiles are differentially affected by the germination processes, with
507 threonine, lysine, arginine and asparagine occurring at higher levels in Mo17 than B73 at the
508 earlier stages of germination (12-h and 24-h post-imbibition), and glutamine levels also
509 increasing in abundance in Mo17 at early stages and in B73 by 36-h post-imbibition.
510 Germination efficiency has been shown to be correlated to differential expression of enzymes

511 involved in aspartate-derived metabolism and, in turn, differential metabolism of specific amino
512 acids (Anzala et al., 2006) as well as nitrogen-derived amino acid metabolism, specifically
513 related to an amino acid-anabolism enzyme, glutamine synthetase (Limami et al., 2002).
514 Moreover, quantitative genetic approaches utilizing B73xMo17 derived germplasm to dissect the
515 genetic basis for germination phenotypes have identified candidate genes involved in amino acid
516 metabolism (Kollipara et al., 2002).

517 A second clear metabolome difference between the two inbreds is in the preferential
518 accumulation of small organic acids in B73 (i.e. malate, pyruvate, fumarate) as compared to
519 Mo17. Interestingly, quantitative genetic analyses of recombinant inbred populations derived
520 from B73 and Mo17 parental inbreds have identified quantitative trait loci associated with
521 germination under both optimal and low temperature conditions. Although numerous candidate
522 genes were identified (> 3000), one encodes a malate dehydrogenase (Hu et al., 2016).
523 Collectively, the observed differences in metabolite accumulation between Mo17 and B73 across
524 early germination provide testable hypotheses regarding their impacts on differential germination
525 efficiency and other germination-related traits that have been shown to differ across maize
526 inbreds.

527 Chromatography-based metabolite profiling generated quantitative data of small
528 molecules, such as sugar monomers, organic acids, amines and amino acids, fatty acids, and
529 sterols, which establish that germinating seeds of the two maize inbreds are readily
530 distinguishable at the level of the expressed metabolome (Fig. 2). While these analyses provided
531 global profiles of the seed metabolomes from which one can generate statistical quantitative
532 correlations among individual metabolite abundances as affected by development and genotype,
533 detailed information on the localization of the metabolites at the cellular level was lost. Further
534 such analyses of seeds micro-dissected to separate different seed organs provided
535 compartmentalization information of the metabolites, and demonstrated that the metabolome of
536 these different organs vary with respect to the developmental program of germination, and is
537 further differentially affected by different genotypes (Fig. 2C and 2D). In general, however,
538 even with the micro-dissected organs, the localization of the metabolites is limited to large,
539 physically separable structures, each of which are made up of a combination of different tissue
540 types with differing metabolic capabilities. Cell-type specific analysis can be done by sorting
541 cells or using laser capture microdissection, but such analysis is not typically applicable for

metabolomic profiling because of the potential metabolite turnover during the laborious sample preparation process. Furthermore, the unknown degree to which these physically separated organs may be cross-contaminated complicates the interpretation of these data. MSI, therefore, offers a convenient means of overcoming the limitations of the chromatography-based metabolite profiling techniques in generating spatially resolved data, with fine-scale localization information in maize seeds at the cellular level.

Combining MALDI-MSI data with chromatography-based analyses allows for more comprehensive coverage of the metabolome beyond that obtainable by either one individually. For example, GC-MS revealed the relative abundance of small sugar molecules (tetroses, pentoses, hexoses and disaccharide), and analysis of micro-dissected seed organs indicated that these small sugars are primarily localized to the embryo as compared to the endosperm, and they also occur in the pericarp and/or aleurone tissues. MSI was only able to visualize the disaccharide species, and that data is in agreement with the distribution determined from the chromatographic analysis of micro-dissected organs. However, MSI provided additional information by successfully visualizing the location of large polysaccharides (Hex_5 to Hex_9), all of which are localized to the starchy endosperm of the seed (Fig. 3A). These results are consistent with the expectation that starch breakdown during germination occurs initially by the action of α- and β-amylase secreted from the scutellum and aleurone. These oligosaccharides are broken down to their constituent glucose units and are transported to and taken up by the scutellum, where they are reassembled into sucrose, the disaccharide likely visualized by MSI (Bewley, 2001; Nonogaki, 2008). The localization of the presumable sucrose disaccharide in the emerging radicle is consistent with the previously reported mobilization of sucrose within the scutellum and subsequent transport to the embryonic axis, specifically to fuel cell elongation in the radicle (Sánchez-Linares et al., 2012).

A similar benefit of combining metabolomic and MSI data is observed when one considers the patterns observed for the different fatty acids and lipid molecular species. GC-MS analysis was limited to being able to detect fatty acids primarily of 16 and 18-carbon chain lengths after derivatization to volatile methyl-esters. In contrast, MALDI-MSI can not only detect these fatty acids without derivatization, but also detect larger non-volatile lipid molecules such as phospholipids, ceramides, and triacylglycerols. Both MSI and GC-MS showed similar fatty acid profiles with minor differences in their relative abundances between the two inbreds.

However, MSI revealed differential localization of the fatty acids dependent on the degrees of unsaturation. Homogeneous distributions were observed within the embryo for palmitate and linoleate, but absences were seen in radicles for oleate and partially for stearate (Fig. 6).

Similar differential patterns of spatial distribution were observed for phospholipids and TAGs depending on their fatty acyl species, in that oleate contributes to the absence in radicles and linoleate contributes to the homogeneous embryonic distributions. For example, fully unsaturated TAG 54:6 (18:2/18:2/18:2) is highly homogeneous throughout the embryo, but becomes absent in the radicle as the degree of saturation increases (Fig. 3B). Phospholipids of PI, PA, and PC show the same trend as TAGs for their absence in the radicle being correlated with the degree of saturation (Fig. 7). PE shows apparently different localization from other phospholipids by having PE molecular species with even-number of unsaturation (36:4, 36:2) evenly distributed throughout the radicle and embryo. However, MS/MS experiments revealed that this is due to the high radicle content of 18:1/18:1 in other 36:2 phospholipids, while PE 36:2 is mostly composed of 18:2/18:0 (Fig. 8B). These results suggest that the heterogeneous distribution of fatty acids dictates the fatty acyl chain dependent differential localization of lipids. Such non-uniform distribution has previously been observed in cotton (Horn et al., 2012) and *Camelina* seeds (Horn et al., 2013); thus, this is not unique to maize, but apparently a more general phenomenon. However, the specifics of the distribution are unique for each species, likely owing to the different anatomy and biological properties of these seeds.

Because plant systems use PC as the substrate for fatty acid desaturation, specifically the FAD2 enzyme that generates 18:2 (Bates et al., 2013; Samuels et al., 2013), we evaluated whether this non-uniform distribution of the unsaturated phospholipids may reflect the distribution of this biosynthetic enzyme. We found that only two of the six FAD2 encoding genes of maize are expressed at this stage of seed germination (namely GRMZM2G056252 and GRMZM2G064701). Moreover, consistent with the hypothesis generated from the MSI data we found that these two *FAD2* genes are preferentially expressed in the radicle tissue relative to the scuttelar tissue, providing a potential explanation for the enrichment of the 18:2-containing lipids in the former.

Ceramide molecular species detected by MSI showed incredibly unique localizations that were significantly different from any other lipid species detected in this work. By directly comparing to PC molecular species, we found that the ceramides are localized to the endosperm

side of the endosperm/scutellum boundary. Previous work has reported the presence of ceramides in maize (Dietrich et al., 2005), as well as in the bran and endosperm of rice grains (Fujino et al., 1985), supporting our observed localization of ceramides in the endosperm of the maize seeds. Although detailed biochemical understanding of the biological functions that ceramides play in plants is relatively poor in comparison to mammalian and fungal organisms (Kolesnick, 2002; Levy and Futerman, 2010), they are thought to be important for plant growth and defense. Inhibition of their biosynthesis by a mycotoxin (Williams et al., 2007) or mutations in the biosynthesis pathway leads to programmed cell death and disease states in plants (Lynch and Dunn, 2004; Markham et al., 2013), whereas induction of their biosynthesis via overexpression of ceramide synthases leads to impacts in biomass accumulation, growth and mycotoxin resistance (Luttgeharm et al., 2015).

In conclusion, this study successfully demonstrated the combined use of chromatography-based metabolite profiling and MALDI-MS based chemical imaging to elucidate the metabolite profile and spatial distribution of metabolites in the complex processes of seed germination in maize. The traditional metabolomics approaches offered comprehensive metabolite coverage of small molecules, which demonstrated that there are significant differences in the metabolite profiles between inbreds during germination, as well as between different seed organ/tissue types of the same inbred. Conversely, MALDI-MSI offers more detailed spatial information on the distribution of the metabolites, especially in terms of unusual localizations of lipids. This study demonstrates the synergy that can be gained by combining these strategies to reveal new insights into complex biological processes that integrate capabilities of different cellular compartments.

Materials and Methods

Seed germination and harvest

Seeds of maize (*Zea mays* L.) inbreds B73 and Mo17 were imbibed and germinated similar to previously described (Liu et al., 2013). Briefly, seeds were placed in deionized water and imbibed while shaking at 300 rpm for 10 minutes. These seeds were then placed embryo side down on moist filter paper in Petri dishes. Plates were incubated in a greenhouse under a diurnal cycle of 15 h light and 9 h dark at 27° C and 24° C, respectively.

Germinating seeds were collected at four time points, 0.2-h, 12-h, 24-h, and 36-h, with the 0.2-h time point corresponding to those taken immediately after 10 minutes of imbibition. At each time point, seeds were collected that appeared similar in terms of their developmental stage. Three seeds chosen for MSI were sectioned longitudinally, and immediately flash frozen in liquid nitrogen and stored at -80° C. From another batch of seeds grown in identical conditions, nine seeds were chosen at each time point for total metabolite and amino acid analysis. Whole seeds were frozen in liquid nitrogen and dried using a vacuum lyophilizer (Labconco Corp., Kansas City, MO); then, three seeds were combined as one biological replicate and pulverized using a Mixer Mill 301(Retsch GmbH, Germany) in 2 ml Eppendorf tubes for total metabolites analysis. A companion set of germinating seeds of similar shapes were collected at the 12-h and 36-h time points, micro-dissected to separate the pericarp and/or aleurone (these two layers could not be separated), tip-cap, embryo and endosperm, and then followed the same lyophilization/pulverization process above for each dissected tissue.

Cryosectioning

Each seed was removed from -80° C storage and quickly placed cut-side down into a plastic cryo-mold (Electron Microscopy Sciences, Hatfield, PA, USA). A warm, 10% w/v gelatin solution was poured into the cryo-mold such that the solution completely covered the seed. The mold was then held over liquid nitrogen until the gelatin became mostly opaque (~1/2 of the gelatin) and then transferred to a -20° C freezer to complete the freezing process.

The frozen gelatin block was then removed from the cryo-mold and mounted on a cryostat chuck. The seed was then cut down to the tissue region of interest (for example, the embryo axis containing the radicle, if the radicle was present in the seed) using a Leica CM1520 cryostat (Leica Biosystems, Buffalo Grove, IL, USA) until the embryonic tissue was visible, following which consecutive 10 μm tissue sections were collected on adhesive tape windows (Leica Biosystems) to preserve structural integrity of the tissue sections. The adhesive windows were then taped face-up onto chilled glass slides and stored at -80° C. A total of 25 sections were taken from each seed and a subset were subjected to either microscopic imaging or MSI analysis.

Microscopy and MALDI imaging preparation

Microscope images of four sections (numbers 5, 11, 17, and 22 of the 25 collected) were obtained using an Olympus SAH-10 stereo-microscope (Olympus Scientific Solutions, Waltham, MA) with an AxioCam HRC and Axio Vision software (Carl Zeiss Inc., Thornwood, NY) to provide finely detailed images. From these images, the highest-quality section was selected based on the clear visualization of developmental stage and section integrity. The sections nearest to this section were chosen for mass spectrometry imaging. The sections selected for MSI were placed on a chilled aluminum plate and then allowed to slowly equilibrate to room temperature under vacuum, preventing condensation and water-soluble metabolite delocalization. Matrix application was performed via sublimation-vapor deposition as previously described (Hankin et al., 2007). Briefly, the sample was attached to the bottom of the sublimation flask condenser, 300 mg of matrix was added to the bottom of the flask, and the flask was sealed and evacuated to ~20 mtorr. The condenser was cooled with a dry ice/acetone slurry. After cooling the condenser, the flask was placed into a pre-heated heating mantle and maintained at a constant temperature (140° C for DAN and DHB, 170° C for 9-AA) for 3-6 minutes until matrix deposition was visible on the tissue surface. After matrix application, tape windows were transferred to a MALDI plate and inserted into the mass spectrometer for MS imaging.

MALDI-MS Imaging

MS imaging data was acquired using a MALDI-linear ion trap (LIT)-Orbitrap mass spectrometer (MALDI-LTQ-Orbitrap Discovery; Thermo Finnigan, San Jose, CA) modified to use an external diode-laser pumped frequency-tripled Nd:YAG laser (355 nm, Elforlight, UVFQ series). For DAN and 9AA in negative ion mode, Orbitrap MS data were acquired using a 100 μm raster size for the *m/z* range of 50-1000. For DHB in positive ion mode, each raster step (100 μm) is broken down into two spiral steps (50 μm each), and Orbitrap MS scans were performed for *m/z* 50-800 and *m/z* 600-1600, respectively. For all imaging runs, the laser spot size was ~40 μm estimated from the burn mark on thin DHB film, except the high-spatial resolution experiment in Figure 5 where the laser spot size was ~10 μm adjusted using a beam expander in the optical beam path. Laser pulse energy and number of shots were optimized for each matrix.

Data analysis and image generation were performed using ImageQuest and Xcalibur software (Thermo). Image normalization was performed for some images and is noted in the figure caption. Mass values and tolerances used to generate images are summarized in Table S1.

For some metabolites, MS images were generated after normalization to the total ion count (TIC) at each pixel (defined by the raster step) to minimize spot-to-spot variation, and the same color scale is used regardless of genotype or germination time point. For most of the metabolites, however, MS images are produced in absolute ion scales without normalization due to the fact that normalization can distort the images for low abundance ions, and the color scheme was arbitrarily adjusted for each image to obtain an image with the highest contrast to display where the metabolite is localized without accentuating background noise.

Separate MS/MS experiments were performed using collision-induced dissociation of the linear ion trap. For m/z 193.051, a collision energy of 100.0 was used with an activation time of 30 ms and an isolation mass window of 0.8 Da. For phospholipid MS/MS, a collision energy of 45.0 was used with an activation time of 30 ms and isolation mass window of 1.0 Da.

Total Metabolites Analysis

Total metabolite extractions were carried out as described previously (Schmidt et al., 2011). Extracts were prepared from ~20 mg of lyophilized and pulverized whole seeds and dissected seed fractions. Each sample was spiked with two internal standards (25 µg of ribitol and 25 µg nonadecanoic acid for polar and non-polar fractions, respectively) and 0.35 ml of hot methanol (60° C) was added and incubated at the same temperature for 10 min, followed by sonication for 10 min at full power. To this slurry, 0.35 ml of chloroform and 0.3 ml of water were added and the mixture was vortexed for 1-3 min. After centrifugation for 5 min at 13,000xg, 200 µl of the upper phase (polar fraction) and 200 µl of the lower phase (non-polar fraction) were separately removed into 2 ml GC-MS vials, and dried in a Speed-Vac concentrator (model SVC 100H, Savant, NY). Both polar and non-polar extracts were analyzed for whole seed samples, and only the polar fractions were analyzed for micro-dissected samples.

Double derivatization via methoximation and silyation was performed to protect ketone functional groups and to increase the volatility of the compounds, respectively. For methoximation, 50 µl of 20 mg/mL methoxyamine hydrochloride dissolved in dry pyridine was added, and the reaction was conducted at 30° C for 1.5 hours with continuous shaking. Silylation was performed by the addition of 70 µL of *N*,*O*-Bis(trimethylsilyl)trifluoroacetamide (BSTFA) with 1% trimethylchlorosilane (TMCS) and incubated at 65° C for 30 min. One microliter of the derivatized samples was injected to GC-MS in splitless mode. GC-MS analysis

was performed using an Agilent 6890 GC interfaced to an Agilent 5973 quadrupole MS with a HP-5ms column (30 m x 0.25 mm x 0.25 μm, Agilent). The temperature gradient was programmed from 70 to 320° C at 5° C/min with helium flow rate at 1.0 mL/min and inlet temperature at 280° C. EI-MS ionization energy was set to 70 eV and the interface temperature was 280° C.

Amino acid analysis

Amino acids analysis was carried out following a method similar to that previously described by Guan et al. (Guan et al., 2015). About 10 mg of lyophilized maize seed powders were extracted with 1 mL of hot water at 85° C for 30 min, and spiked with 10 μM butylamine internal standard. The samples were briefly centrifuged for 5 min, passed through a syringe filter with 0.2 μm pore size, and subjected to LC-fluorescence amino acid analysis with pre-column derivatization of primary amino acids with o-phthaldialdehyde (OPA).

LC-fluorescence analysis was performed using an Agilent 1110 HPLC with a fluorescence detector (FLD) with a Hypersil ODS C18 reverse phase column (250mm x 4mm, 5μm; Thermo). Excitation and emission wavelengths for FLD were set at 337 nm and 454 nm, respectively. Solvent system used were buffer A (10% methanol (MeOH) in 10 mM NaH_2PO_4, pH 7.3), buffer B (80% MeOH in 10 mM NaH_2PO_4, pH 7.3), and OPA solution (12.25 mg OPA in 312.5 μL MeOH, 6 mL 0.4 M borate buffer and 19.22 μL mercaptoethanol). The pre-column OPA derivatization reaction was achieved using an in-loop-reaction program. Solvent program was a linear gradient from 100% buffer A to 100% buffer B in 46 min at flow rate of 1 ml/min. Amino acid standard mixture included butylamine and 18 of the 20 proteogenic amino acids, at the concentration of 10mM each. Cys and Pro cannot be analyzed by this method and were not included as standards. The amino acid standard mixture was used to calculate the response factors for the detector, and butylamine was used to generate a standard curve.

Data Analysis

Three biological replicates were used for GC or LC analysis of the extracts. Those compounds that were observed in two or three datasets were subjected to statistical analysis and reported here. For those compounds observed only in two data sets, the missing values were replaced by 1/3 of the estimated minimum value. Log2 ratio plots were calculated for each

metabolite as previously described (Quanbeck et al., 2012). The raw data and averages and standard error calculations were determined from three biological replicates and are available in the PMR database and Supplemental Tables (i.e, Table S2, S3 and S4) respectively. Student t-test were used to calculate p-values.

The GC/MS data files were deconvoluted and searched against an in-house MS-library and NIST 14 Mass Spectral Library using NIST AMDIS software (Stein, 1999). Total metabolite analysis results obtained with GC-MS and amino acid analysis from LC-fluorescence are publicly available in the PMR database (http://metnetdb.org/PMR/)(Hur et al., 2013). They are available from the site in the name of 'Seed Germination' under the species of 'Zea mays'.

RNA extraction and quantitative PCR

Embryos were micro-dissected from germinating seeds at different times after imbibition, and the scutellar tissue was separated from the radicle. The flash frozen tissues were pulverized, and RNA was extracted (Wang et al., 2012). The isolated RNA preparations were treated with DNase (Ambion), and 8 µg of RNA was reverse-transcribed using *Double Primed RNA to cDNA EcoDry Premix* (Clontech, Mountain View, CA). *FAD2* gene sequences were identified using the Gramene (www.gramene.org) and Maize genome (www.maizegdb.org) databases. Primer pairs for qRT-PCR were designed and computationally tested for specificity using Primer-BLAST (Ye et al., 2012). PCR was performed with a StepOnePlus Real-Time PCR System (Applied Biosystems). The PCR reaction mixture contained cDNA template, primer mix and SYBR® Select Master Mix (Applied Biosystems) in a final volume of 20 µl. Annealing temperature in the PCR reaction was 58°C using gene-specific oligonucleotide primers (Table S6). The Ct ($2^{-\Delta\Delta Ct}$) method (Livak and Schmittgen, 2001) was used to analyze the comparative expression of each *FAD2* mRNA, using the expression of the ubiquitin mRNA (GenBank Accession Number: BT018032) as the internal control.

Supplemental Materials

Figure S1. Log-ratio plots comparing the amino acids of Mo17 and B73 maize inbred seeds.

Figure S2. Log-ratio plots comparing the metabolome of different organ tissues of Mo17 and B73 maize inbred seeds.

Figure S3. Compartmentalization of total amino acids in maize seeds.

Figure S4. MS/MS of *m/z* 193.051.

Figure S5. Malic acid images and GC-MS data from micro-dissected seed organs.

Figure S6. GC-MS data for palmitic, linoleic, oleic and stearic acids.

Figure S7. MS images for PE, PA, PI, and PC species over all four germination time points.

Figure S8. Four-step imaging scheme for MS/MS of lipid species

Figure S9. MS/MS of PA 36:3 and PE 36:3 from the radicle of a Mo17 seed.

Figure S10. Images for three additional ceramide species not shown in Figure 8.

Table S1. List of all *m/z* values and parameters used for image generation in this work.

Table S2. Metabolite abundance data detected from whole seed via GC-MS analysis

Table S3. Amino acid data detected from whole seed via LC-fluorescence

Table S4. Metabolite abundance data detected from micro-dissected seed organs analyzed by GC-MS.

Table S5. Normalized expression level of six individual *FAD2* encoding mRNAs in radicle tissues relative to scutellar tissues of germinating seeds from inbred B73 and Mo17.

Table S6. List of primer sequences used for qRT-PCR analysis

Acknowledgments

This work was supported by the US Department of Energy (DOE), Office of Basic Energy Sciences, Division of Chemical Sciences, Geosciences, and Biosciences. Metabolomics analyses were conducted at the Iowa State University WM Keck Metabolomics Research Laboratory, and we acknowledge Ann M. Perera for her expert advice. The Ames Laboratory is operated by Iowa State University under DOE Contract DE-AC02-07CH11358.

Figure Legends

Fig. 1. Illustration of experimental workflow. **(A)** Sample preparation: Seeds were germinated in a petri dish and quenched at the desired time point with liquid nitrogen (LN_2). Some samples were selected for metabolite profiling analysis. The remaining samples were cryo-sectioned at 10 µm thickness for microscopic and MSI analysis. **(B)** MSI data acquisition and analysis: The laser was rastered across the tissue sample, collecting a spectrum at every x-y position. Resulting mass spectra were evaluated and MS images were generated for individual ions at selected *m/z* values.

Fig. 2. Log-ratio plot comparison **(A)** and Venn-diagram representations of the differential metabolomes between Mo17 and B73 maize inbred of whole seeds **(B)** and micro-dissected organs from seeds at 12-h **(C)** and 36-h **(D)** post-imbibition. In the log-ratio plots the x-axis plots log-transformed relative abundance ratio of each metabolite in Mo17 vs B73. The y-axis plots the individual metabolites (162 analytes, 63 chemically defined), and the order of the metabolites on the y-axis is identical and ordered from the lowest to the highest value on the x-axis as determined for the 12-h post-imbibition time point. The arrows identify amino acids or those metabolites also analyzed by MSI. Glyc3P = glycerol 3-phosphate; FA = Fatty acid. The Venn-diagram in panel B represents the distribution of metabolites that are differentially expressed between Mo17 and B73 seeds ($p<0.05$) among the four post-imbibition time points. The Venn diagrams in panels C and D show metabolites that are differentially expressed between Mo17 and B73 seeds ($p<0.05$) in micro-dissected organs from germinating seeds at 12-h and 36-h post-imbibition. The identity of the inbred and the number of the metabolites that occur at higher levels is represented by the labels "inbred(x)".

Fig. 3. MSI images of **(A)** hexose polysaccharides, **(B)** triacylglycerols, and **(C)** amino acids in germinating seeds. All ions were detected in positive ion mode with DHB as the matrix. Large polysaccharides were detected as potassium adducts of water loss, $[M\text{-}H_2O+K]^+$, likely due to in-source fragmentation during MALDI-MS data acquisition. Disaccharide and triacylglycerols were detected as potassium adducts, $[M+K]^+$, and amino acids were detected as protonated ions, $[M+H]^+$. Scale bar: 1 mm.

Fig. 4. **(A)** MSI of three compounds uniquely localized to the perimeter of the seed. Images were acquired in negative ion mode with DAN as matrix. No normalization was applied to these images. Scale bar: 1 mm. **(B)** Optical microscopic (Top) and MS (Bottom) images of the

pericarp and aleurone layers of a B73 maize seed with 24-h post-imbibition. Morphological features are labeled on the images. G: gelatin embedding medium. P: pericarp. A: aleurone. E: endosperm. **(C)** Overlay of optical and MS images in the panel B. MS images were obtained with DAN as the matrix in negative mode. MS images in the panel B and C are ferulate (red), malate (blue), and PI 34:2 (green). All analytes were detected as deprotonated species, $[M-H]^-$. Scale bar: 100 μm.

Fig. 5. Distribution of hexose phosphate (Hex6P), glycerol phosphate (GlycP), and citrate/isocitrate. Phosphorylated metabolites are detected as deprotonated water-loss species, $[M-H_2O-H]^-$, in negative ion mode with DAN as matrix. Citrate/isocitrate is detected as a deprotonated species, $[M-H]^-$, in negative ion mode with 9AA as matrix. Scale bar: 1 mm.

Fig. 6. Distribution of fatty acid species. All ions were detected as the deprotonated species, $[M-H]^-$, in negative ion mode with 9AA as the matrix. Scale bar: 1 mm. Stearate has some contamination from vacuum pump oil.

Fig. 7. Distribution and species analysis of various phospholipids. **(A)** Distribution of 16 different phospholipid molecular species in germinating seeds (36-h post imbibition). PE, PA, and PI are observed as deprotonated species, $[M-H]^-$, with DAN as the matrix in negative ion mode. PC is observed as a potassium adduct, $[M+K]^+$, with DHB matrix in positive ion mode. To allow direct comparisons, the optical images of the seeds were obtained from the adjacent cross-sections to those used to generate the MS images. Scale bar: 1 mm. Arrows in the radicle and scutellum regions of the embryo indicate the areas used to generate averaged mass spectra, from which semi-quantitative data of the phospholipids were gathered (see panels B and C). **(B)** Phospholipid ion signals in the radicle region normalized relative to the signals obtained from the scutellum. **(C)** Percentage of each molecular species within each phospholipid class in the radicle region.

Fig. 8. MS/MS analysis of phospholipid species. **(A)** MS/MS spectra of PA 36:2 (top) and PE 36:2 (bottom) obtained from the radicle of a Mo17 inbred seed (24-hr post-imbibition). **(B)** Fatty acyl composition of different molecular species of PA 36:2 and PE 36:2, in the scutellum and radicle region of Mo17 and B73 seeds (24-hr post-imbibition).

872 **Fig. 9.** Relative FAD2 expression in radicle and scutellar tissues of germinating maize seeds.
873 FAD2 transcript levels encoded by GRMZM2G056252 (■, □) and GRMZM2G064701 (▲,
874 △) were determined in RNA isolated from the radicle and scutellar tissues of germinating seeds
875 from the inbreds B73 (—) and Mo17 (—)12-48-h post-imbibition. The expression of FAD2
876 transcripts was calculated by $2^{-(\Delta\Delta C_T)}$, using the ubiquitin mRNA (GenBank Accession Number:
877 BT018032) as the internal control. Expression of each FAD2 transcript is normalized relative to
878 the level found in the scutellar tissue.

879 **Fig. 10.** Distribution of ceramide species. **(A)** Distributions of two ceramide molecular species
880 (Cer d42:1, Cer t42:0). Both are detected as protonated species, $[M+H]^+$, in positive ion mode
881 with DHB as the matrix. Scale bar: 1 mm. **(B)** Combined images of PC 34:2 (green) and
882 ceramide d42:1 (red) in a B73 inbred seed at 12-h post-imbibition.

883

884

References:

Anzala F, Morère-Le Paven M-C, Fournier S, Rondeau D, Limami AM (2006) Physiological and molecular aspects of aspartate-derived amino acid metabolism during germination and post-germination growth in two maize genotypes differing in germination efficiency. Journal of experimental botany **57:** 645-653

Bates PD, Stymne S, Ohlrogge J (2013) Biochemical pathways in seed oil synthesis. Current opinion in plant biology **16:** 358-364

Bernier AM, Ballance GM (1993) INDUCTION AND SECRETION OF ALPHA-AMYLASE, (1- 3),(1- 4)-BETA-GLUCANASE, AND (1- 3)-BETA-GLUCANASE ACTIVITIES IN GIBBERELLIC-ACID AND CACL2-TREATED HALF SEEDS AND ALEURONES OF WHEAT. Cereal Chemistry **70:** 127-132

Bewley JD (1997) Seed germination and dormancy. The plant cell **9:** 1055

Bewley JD (2001) Seed Germination and Reserve Mobilization. eLS

Bewley JD, Bradford K, Hilhorst H (2012) Seeds: physiology of development, germination and dormancy. Springer Science & Business Media

Chrispeels MJ, Varner J (1967) Hormonal control of enzyme synthesis: on the mode of action of gibberellic acid and abscisin in aleurone layers of barley. Plant physiology **42:** 1008-1016

Dante RA, Larkins BA, Sabelli PA (2015) Cell cycle control and seed development. Advances in Seed Biology**:** 21

Dietrich CR, Perera M, D Yandeau- Nelson M, Meeley RB, Nikolau BJ, Schnable PS (2005) Characterization of two GL8 paralogs reveals that the 3- ketoacyl reductase component of fatty acid elongase is essential for maize (Zea mays L.) development. The Plant Journal **42:** 844-861

Feenstra AD, Hansen RL, Lee YJ (2015) Multi-matrix, dual polarity, tandem mass spectrometry imaging strategy applied to a germinated maize seed: toward mass spectrometry imaging of an untargeted metabolome. Analyst **140:** 7293-7304

Fincher GB (1989) Molecular and cellular biology associated with endosperm mobilization in germinating cereal grains. Annual review of plant biology **40:** 305-346

Firenzuoli A, Vanni P, Ramponi G, Baccari V (1968) Changes in enzyme levels during germination of seeds of Triticum durum. Plant physiology **43:** 260-264

Frank T, Scholz B, Peter S, Engel K-H (2011) Metabolite profiling of barley: Influence of the malting process. Food chemistry **124:** 948-957

Fu Y, Wen T-J, Ronin YI, Chen HD, Guo L, Mester DI, Yang Y, Lee M, Korol AB, Ashlock DA (2006) Genetic dissection of intermated recombinant inbred lines using a new genetic map of maize. Genetics **174:** 1671-1683

Fujino Y, Ohnishi M, Ito S (1985) Molecular species of ceramide and mono-, di-, tri-, and tetraglycosylceramide in bran and endosperm of rice grains. Agricultural and biological chemistry **49:** 2753-2762

Guan X, Chen H, Abramson A, Man H, Wu J, Yu O, Nikolau BJ (2015) A phosphopantetheinyl transferase that is essential for mitochondrial fatty acid biosynthesis. The Plant Journal **84:** 718-732

Hankin JA, Barkley RM, Murphy RC (2007) Sublimation as a method of matrix application for mass spectrometric imaging. Journal of the American Society for Mass Spectrometry **18:** 1646-1652

He M, Zhu C, Dong K, Zhang T, Cheng Z, Li J, Yan Y (2015) Comparative proteome analysis of embryo and endosperm reveals central differential expression proteins involved in wheat seed germination. BMC plant biology **15:** 1

Hirsch CN, Foerster JM, Johnson JM, Sekhon RS, Muttoni G, Vaillancourt B, Peñagaricano F, Lindquist E, Pedraza MA, Barry K (2014) Insights into the maize pan-genome and pan-transcriptome. The Plant Cell **26:** 121-135

Horn PJ, Korte AR, Neogi PB, Love E, Fuchs J, Strupat K, Borisjuk L, Shulaev V, Lee Y-J, Chapman KD (2012) Spatial Mapping of Lipids at Cellular Resolution in Embryos of Cotton. The Plant Cell **24:** 622-636

Horn PJ, Silva JE, Anderson D, Fuchs J, Borisjuk L, Nazarenus TJ, Shulaev V, Cahoon EB, Chapman KD (2013) Imaging heterogeneity of membrane and storage lipids in transgenic Camelina sativa seeds with altered fatty acid profiles. Plant Journal **76:** 138-150

Hou W, Zhou H, Khalil MB, Seebun D, Bennett SA, Figeys D (2011) Lyso- form fragment ions facilitate the determination of stereospecificity of diacyl glycerophospholipids. Rapid Communications in Mass Spectrometry **25:** 205-217

Hu S, Lübberstedt T, Zhao G, Lee M (2016) QTL Mapping of Low-Temperature Germination Ability in the Maize IBM Syn4 RIL Population. PloS one **11:** e0152795

Hur M, Campbell AA, Almeida-de-Macedo M, Li L, Ransom N, Jose A, Crispin M, Nikolauh BJ, Wurtele ES (2013) A global approach to analysis and interpretation of metabolic data for plant natural product discovery. Natural Product Reports **30:** 565-583

Ingle J, Beevers L, Hageman R (1964) Metabolic changes associated with the germination of corn. I. Changes in weight and metabolites and their redistribution in the embryo axis, scutellum, and endosperm. Plant physiology **39:** 735

Kaspar S, Peukert M, Svatos A, Matros A, Mock HP (2011) MALDI- imaging mass spectrometry–An emerging technique in plant biology. Proteomics **11:** 1840-1850

Kolesnick R (2002) The therapeutic potential of modulating the ceramide/sphingomyelin pathway. The Journal of clinical investigation **110:** 3-8

Kollipara KP, Saab IN, Wych RD, Lauer MJ, Singletary GW (2002) Expression profiling of reciprocal maize hybrids divergent for cold germination and desiccation tolerance. Plant Physiology **129:** 974-992

Korte AR, Yandeau-Nelson MD, Nikolau BJ, Lee YJ (2015) Subcellular-level resolution MALDI-MS imaging of maize leaf metabolites by MALDI-linear ion trap-Orbitrap mass spectrometer. Analytical and bioanalytical chemistry **407:** 2301-2309

Lai J, Li R, Xu X, Jin W, Xu M, Zhao H, Xiang Z, Song W, Ying K, Zhang M (2010) Genome-wide patterns of genetic variation among elite maize inbred lines. Nature genetics **42:** 1027-1030

Larson G, Piperno DR, Allaby RG, Purugganan MD, Andersson L, Arroyo-Kalin M, Barton L, Vigueira CC, Denham T, Dobney K (2014) Current perspectives and the future of

967 domestication studies. Proceedings of the National Academy of Sciences **111:** 6139-
968 6146
969 **Lee YJ, Perdian DC, Song Z, Yeung ES, Nikolau BJ** (2012) Use of mass spectrometry for imaging
970 metabolites in plants. Plant Journal **70:** 81-95
971 **Leonova S, Grimberg Å, Marttila S, Stymne S, Carlsson AS** (2010) Mobilization of lipid reserves
972 during germination of oat (Avena sativa L.), a cereal rich in endosperm oil. Journal of
973 experimental botany **61:** 3089-3099
974 **Levy M, Futerman AH** (2010) Mammalian ceramide synthases. IUBMB life **62:** 347-356
975 **Limami AM, Rouillon C, Glevarec G, Gallais A, Hirel B** (2002) Genetic and physiological analysis
976 of germination efficiency in maize in relation to nitrogen metabolism reveals the
977 importance of cytosolic glutamine synthetase. Plant Physiology **130:** 1860-1870
978 **Liu W-Y, Chang Y-M, Chen SC-C, Lu C-H, Wu Y-H, Lu M-YJ, Chen D-R, Shih AC-C, Sheue C-R,**
979 **Huang H-C** (2013) Anatomical and transcriptional dynamics of maize embryonic leaves
980 during seed germination. Proceedings of the National Academy of Sciences **110:** 3979-
981 3984
982 **Livak KJ, Schmittgen TD** (2001) Analysis of Relative Gene Expression Data Using Real-Time
983 Quantitative PCR and the 2−ΔΔCT Method. Methods **25:** 402-408
984 **Lu H, Bernardo R** (2001) Molecular marker diversity among current and historical maize
985 inbreds. Theoretical and Applied Genetics **103:** 613-617
986 **Luttgeharm KD, Chen M, Mehra A, Cahoon RE, Markham JE, Cahoon EB** (2015) Overexpression
987 of Arabidopsis ceramide synthases differentially affects growth, sphingolipid
988 metabolism, programmed cell death, and mycotoxin resistance. Plant physiology **169:**
989 1108-1117
990 **Lynch DV, Dunn TM** (2004) An introduction to plant sphingolipids and a review of recent
991 advances in understanding their metabolism and function. New phytologist **161:** 677-
992 702
993 **Markham JE, Lynch DV, Napier JA, Dunn TM, Cahoon EB** (2013) Plant sphingolipids: function
994 follows form. Current opinion in plant biology **16:** 350-357
995 **McDonnell LA, Heeren R** (2007) Imaging mass spectrometry. Mass spectrometry reviews **26:**
996 606-643
997 **McDonnell LA, Heeren RMA** (2007) Imaging mass spectrometry. Mass Spectrometry Reviews
998 **26:** 606-643
999 **Munamava MR, Goggi AS, Pollak L** (2004) Seed quality of maize inbred lines with different
1000 composition and genetic backgrounds. Crop science **44:** 542-548
1001 **Nonogaki H** (2008) Seed germination and reserve mobilization. eLS
1002 **Petryszak R, Keays M, Tang YA, Fonseca NA, Barrera E, Burdett T, Füllgrabe A, Fuentes AM-P,**
1003 **Jupp S, Koskinen S, Mannion O, Huerta L, Megy K, Snow C, Williams E, Barzine M,**
1004 **Hastings E, Weisser H, Wright J, Jaiswal P, Huber W, Choudhary J, Parkinson HE,**
1005 **Brazma A** (2016) Expression Atlas update—an integrated database of gene and protein
1006 expression in humans, animals and plants. Nucleic Acids Research **44:** D746-D752
1007 **Quanbeck SMM, Brachova L, Campbell AA, Guan X, Perera A, He K, Rhee SY, Bais P, Dickerson**
1008 **J, Dixon P** (2012) Metabolomics as a hypothesis-generating functional genomics tool for
1009 the annotation of Arabidopsis thaliana genes of “unknown function”. Frontiers in plant
1010 science **3:** 15

Römisch-Margl L, Spielbauer G, Schützenmeister A, Schwab W, Piepho H-P, Genschel U, Gierl A (2010) Heterotic patterns of sugar and amino acid components in developing maize kernels. Theoretical and Applied Genetics **120:** 369-381

Samuels KMS, Wada H, Welti R, Xu C, Zallot R, Ohlrogge J (2013) Acyl-lipid metabolism. The Arabidopsis Book **1:** 70

Sánchez-Linares L, Gavilanes-Ruíz M, Díaz-Pontones D, Guzmán-Chávez F, Calzada-Alejo V, Zurita-Villegas V, Luna-Loaiza V, Moreno-Sánchez R, Bernal-Lugo I, Sánchez-Nieto S (2012) Early carbon mobilization and radicle protrusion in maize germination. Journal of experimental botany**:** ers130

Schmidt MA, Barbazuk WB, Sandford M, May G, Song Z, Zhou W, Nikolau BJ, Herman EM (2011) Silencing of soybean seed storage proteins results in a rebalanced protein composition preserving seed protein content without major collateral changes in the metabolome and transcriptome. Plant Physiology **156:** 330-345

Schnable PS, Ware D, Fulton RS, Stein JC, Wei F, Pasternak S, Liang C, Zhang J, Fulton L, Graves TA (2009) The B73 maize genome: complexity, diversity, and dynamics. science **326:** 1112-1115

Sen TZ, Harper LC, Schaeffer ML, Andorf CM, Seigfried TE, Campbell DA, Lawrence CJ (2010) Choosing a genome browser for a Model Organism Database: surveying the Maize community. Database-the Journal of Biological Databases and Curation

Shu X-L, Frank T, Shu Q-Y, Engel K-H (2008) Metabolite profiling of germinating rice seeds. Journal of agricultural and food chemistry **56:** 11612-11620

Springer NM, Ying K, Fu Y, Ji T, Yeh C-T, Jia Y, Wu W, Richmond T, Kitzman J, Rosenbaum H (2009) Maize inbreds exhibit high levels of copy number variation (CNV) and presence/absence variation (PAV) in genome content. PLoS Genet **5:** e1000734

Stein SE (1999) An integrated method for spectrum extraction and compound identification from gas chromatography/mass spectrometry data. Journal of the American Society for Mass Spectrometry **10:** 770-781

Swanson-Wagner RA, Eichten SR, Kumari S, Tiffin P, Stein JC, Ware D, Springer NM (2010) Pervasive gene content variation and copy number variation in maize and its undomesticated progenitor. Genome research **20:** 1689-1699

Toue S, Sugiura Y, Kubo A, Ohmura M, Karakawa S, Mizukoshi T, Yoneda J, Miyano H, Noguchi Y, Kobayashi T (2014) Microscopic imaging mass spectrometry assisted by on‐tissue chemical derivatization for visualizing multiple amino acids in human colon cancer xenografts. Proteomics **14:** 810-819

Troyer AF (2004) Persistent and popular germplasm in seventy centuries of corn evolution. Corn: Origin, History, and Production. John Wiley & Sons, Hoboken, NJ**:** 133-231

Troyer AF (2009) Development of hybrid corn and the seed corn industry. *In* Handbook of maize. Springer, pp 87-114

van Hove ERA, Smith DF, Heeren RM (2010) A concise review of mass spectrometry imaging. Journal of Chromatography A **1217:** 3946-3954

Vroh Bi I, McMullen M, Sanchez-Villeda H, Schroeder S, Gardiner J, Polacco M, Soderlund C, Wing R, Fang Z, Coe E (2006) Single nucleotide polymorphisms and insertion–deletions

for genetic markers and anchoring the maize fingerprint contig physical map. Crop science **46:** 12-21

Wang G, Wang G, Zhang X, Wang F, Song R (2012) Isolation of High Quality RNA from Cereal Seeds Containing High Levels of Starch. Phytochemical Analysis **23:** 159-163

Williams LD, Glenn AE, Zimeri AM, Bacon CW, Smith MA, Riley RT (2007) Fumonisin disruption of ceramide biosynthesis in maize roots and the effects on plant development and Fusarium verticillioides-induced seedling disease. Journal of agricultural and food chemistry **55:** 2937-2946

Ye J, Coulouris G, Zaretskaya I, Cutcutache I, Rozen S, Madden TL (2012) Primer-BLAST: A tool to design target-specific primers for polymerase chain reaction. BMC Bioinformatics **13:** 134

Zavalin A, Yang J, Caprioli R (2013) Laser Beam Filtration for High Spatial Resolution MALDI Imaging Mass Spectrometry. Journal of The American Society for Mass Spectrometry **24:** 1153-1156

Zeeman SC, Delatte T, Messerli G, Umhang M, Stettler M, Mettler T, Streb S, Reinhold H, Kötting O (2007) Starch breakdown: recent discoveries suggest distinct pathways and novel mechanisms. *In*, Vol 34. CSIRO Publishing, Functional Plant Biology, pp 465-473

Zhang M, Fan J, Taylor DC, Ohlrogge JB (2009) DGAT1 and PDAT1 acyltransferases have overlapping functions in Arabidopsis triacylglycerol biosynthesis and are essential for normal pollen and seed development. The Plant Cell **21:** 3885-3901

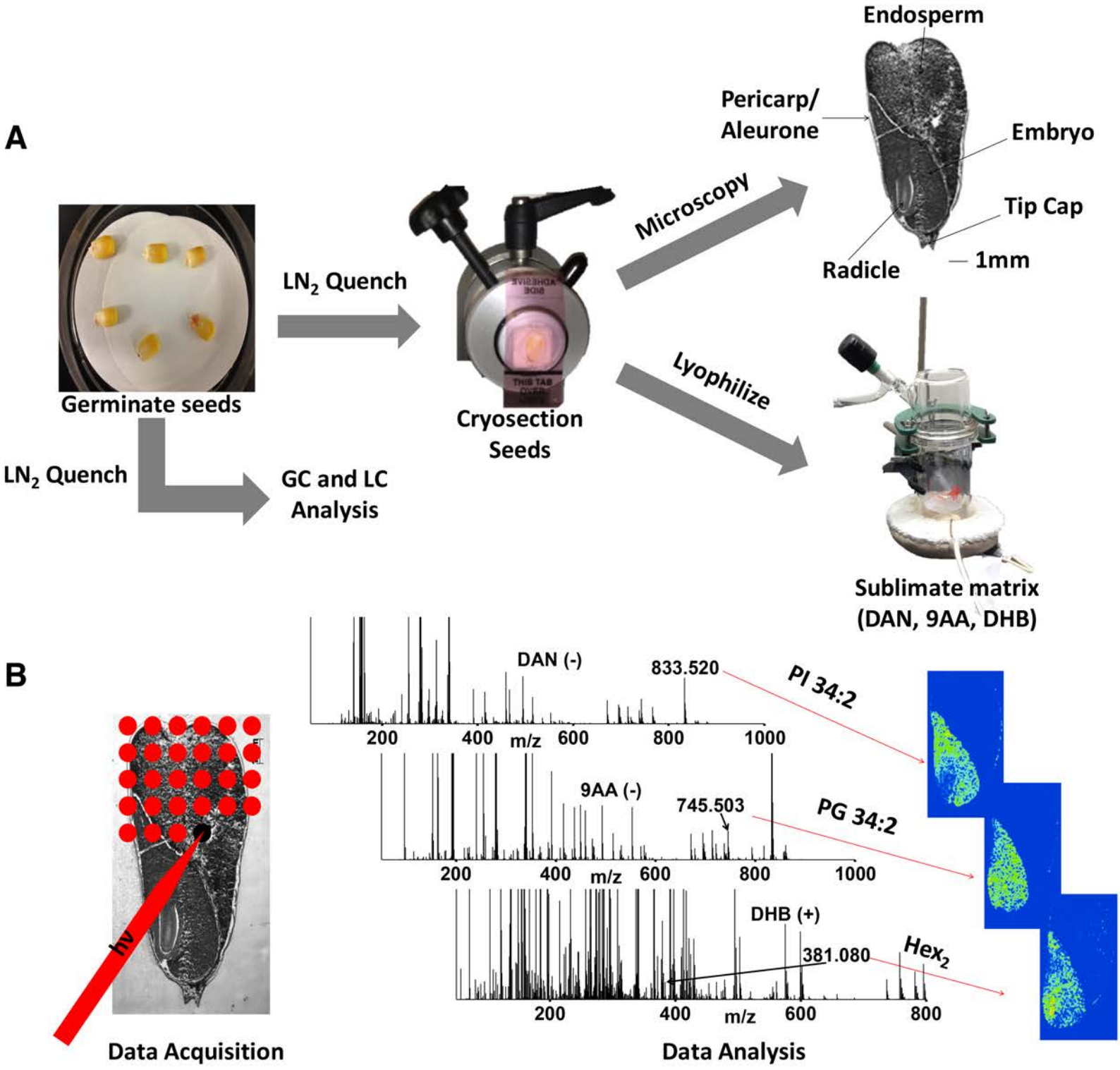

Fig. 1. Illustration of experimental workflow. **(A)** Sample preparation: Seeds were germinated in a petri dish and quenched at the desired time point with liquid nitrogen (LN_2). Some samples were selected for metabolite profiling analysis. The remaining samples were cryo-sectioned at 10 µm thickness for microscopic and MSI analysis. **(B)** MSI data acquisition and analysis: The laser was rastered across the tissue sample, collecting a spectrum at every x-y position. Resulting mass spectra were evaluated and MS images were generated for individual ions at selected *m/z* values.

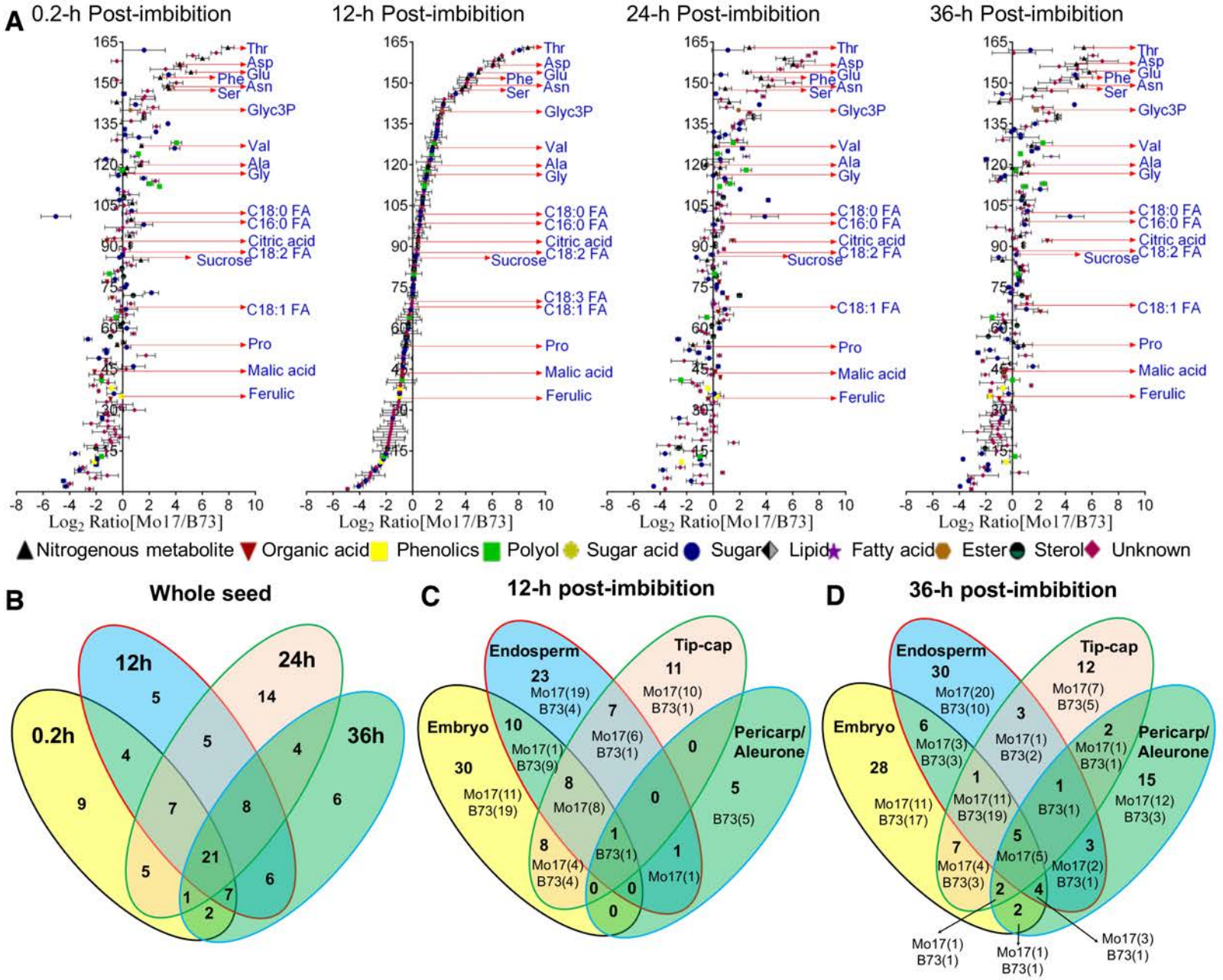

Fig. 2. Log-ratio plot comparison **(A)** and Venn-diagram representations of the differential metabolomes between Mo17 and B73 maize inbred of whole seeds **(B)** and micro-dissected organs from seeds at 12-h **(C)** and 36-h **(D)** post-imbibition. In the log-ratio plots the x-axis plots log-transformed relative abundance ratio of each metabolite in Mo17 vs B73. The y-axis plots the individual metabolites (162 analytes, 63 chemically defined), and the order of the metabolites on the y-axis is identical and ordered from the lowest to the highest value on the x-axis as determined for the 12-h post-imbibition time point. The arrows identify amino acids or those metabolites also analyzed by MSI. Glyc3P = glycerol 3-phosphate; FA = Fatty acid. The Venn-diagram in panel B represents the distribution of metabolites that are differentially expressed between Mo17 and B73 seeds ($p<0.05$) among the four post-imbibition time points. The Venn diagrams in panels C and D show metabolites that are differentially expressed between Mo17 and B73 seeds ($p<0.05$) in micro-dissected organs from germinating seeds at 12-h and 36-h post-imbibition. The identity of the inbred and the number of the metabolites that occur at higher levels is represented by the Babels-in-Dreadx's.

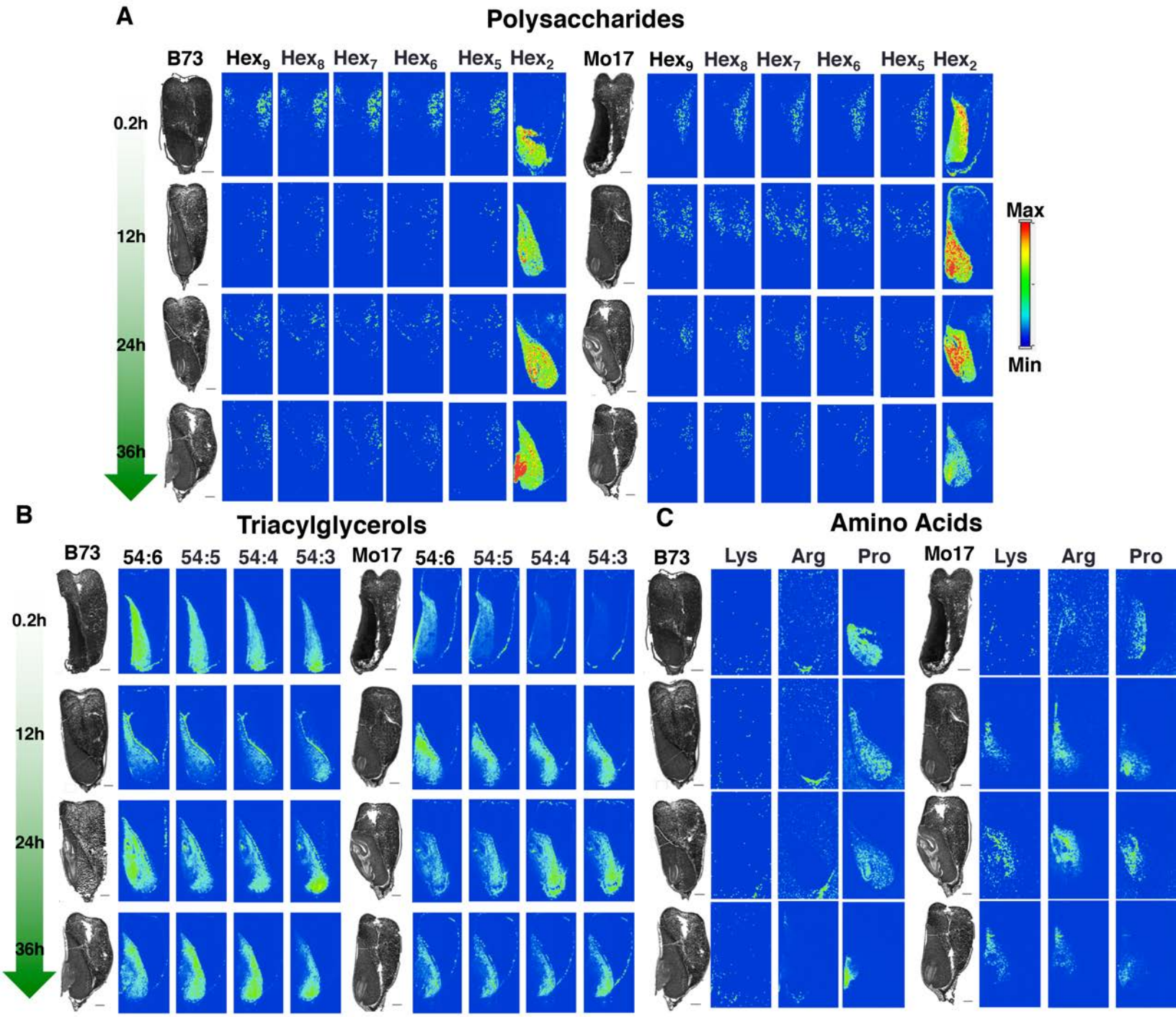

Fig. 3. MSI images of **(A)** hexose polysaccharides, **(B)** triacylglycerols, and **(C)** amino acids in germinating seeds. All ions were detected in positive ion mode with DHB as the matrix. Large polysaccharides were detected as potassium adducts of water loss, $[M\text{-}H_2O+K]^+$, likely due to in-source fragmentation during MALDI-MS data acquisition. Disaccharide and triacylglycerols were detected as potassium adducts, $[M+K]^+$, and amino acids were detected as protonated ions, $[M+H]^+$. Scale bar: 1 mm.

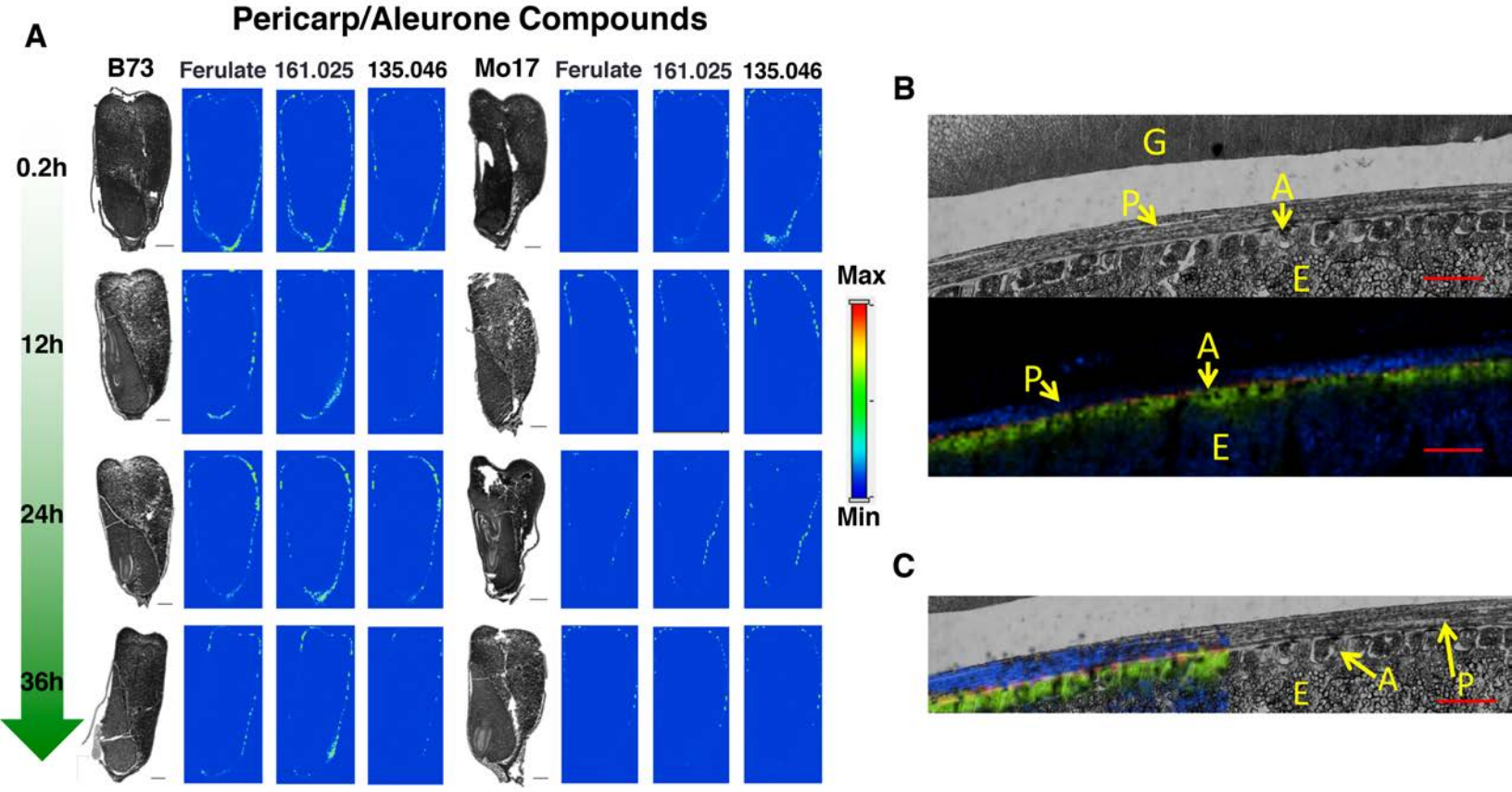

Fig. 4. **(A)** MSI of three compounds uniquely localized to the perimeter of the seed. Images were acquired in negative ion mode with DAN as matrix. No normalization was applied to these images. Scale bar: 1 mm. **(B)** Optical microscopic (Top) and MS (Bottom) images of the pericarp and aleurone layers of a B73 maize seed with 24-h post-imbibition. Morphological features are labeled on the images. G: gelatin embedding medium. P: pericarp. A: aleurone. E: endosperm. **(C)** Overlay of optical and MS images in the panel B. MS images were obtained with DAN as the matrix in negative mode. MS images in the panel B and C are ferulate (red), malate (blue), and PI 34:2 (green). All analytes were detected as deprotonated species, $[M-H]^-$. Scale bar: 100 μm.

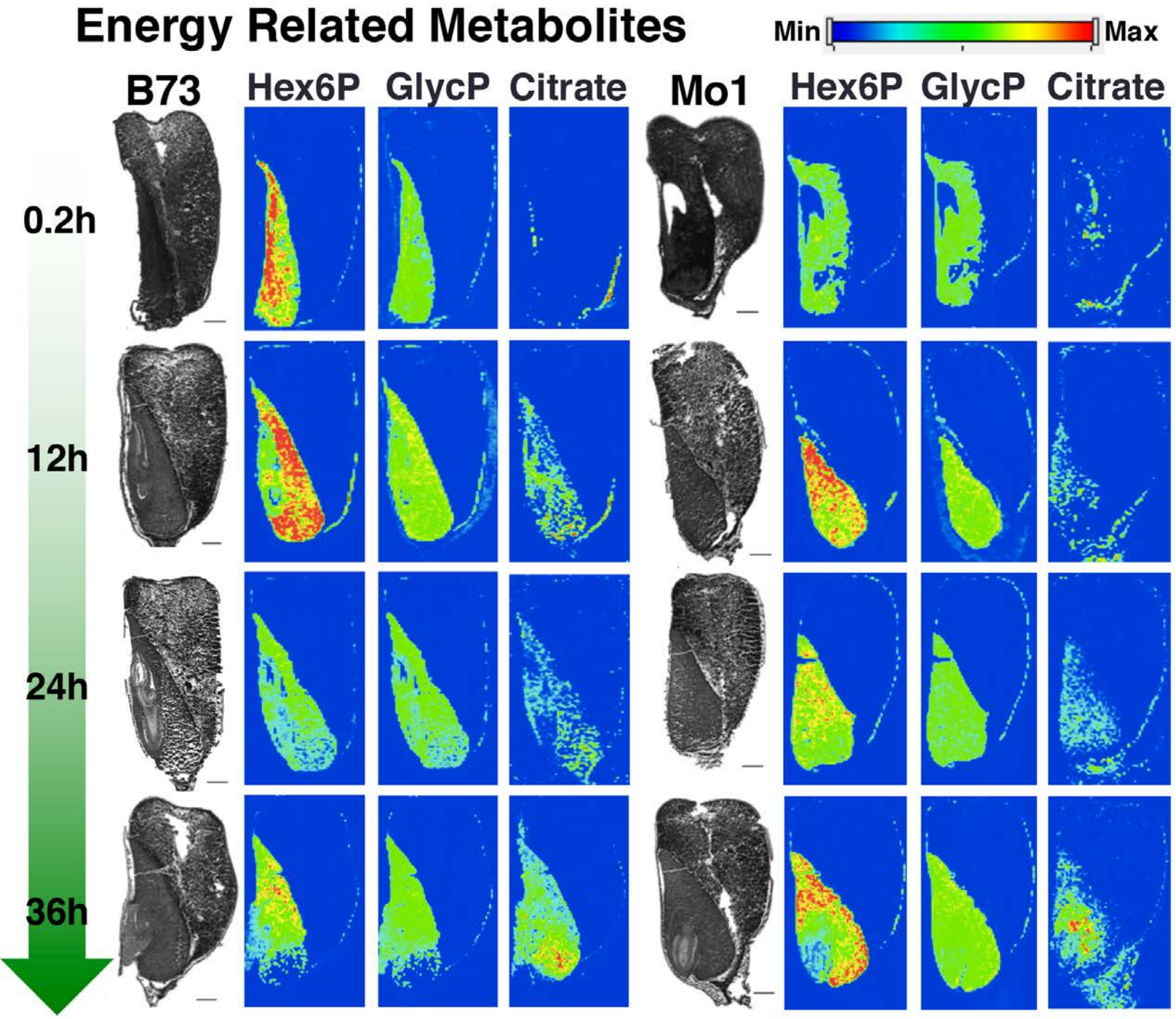

Fig. 5. Distribution of hexose phosphate (Hex6P), glycerol phosphate (GlycP), and citrate/isocitrate. Phosphorylated metabolites are detected as deprotonated water-loss species, $[M\text{-}H_2O\text{-}H]^-$, in negative ion mode with DAN as matrix. Citrate/isocitrate is detected as a deprotonated species, $[M\text{-}H]^-$, in negative ion mode with 9AA as matrix. Scale bar: 1 mm.

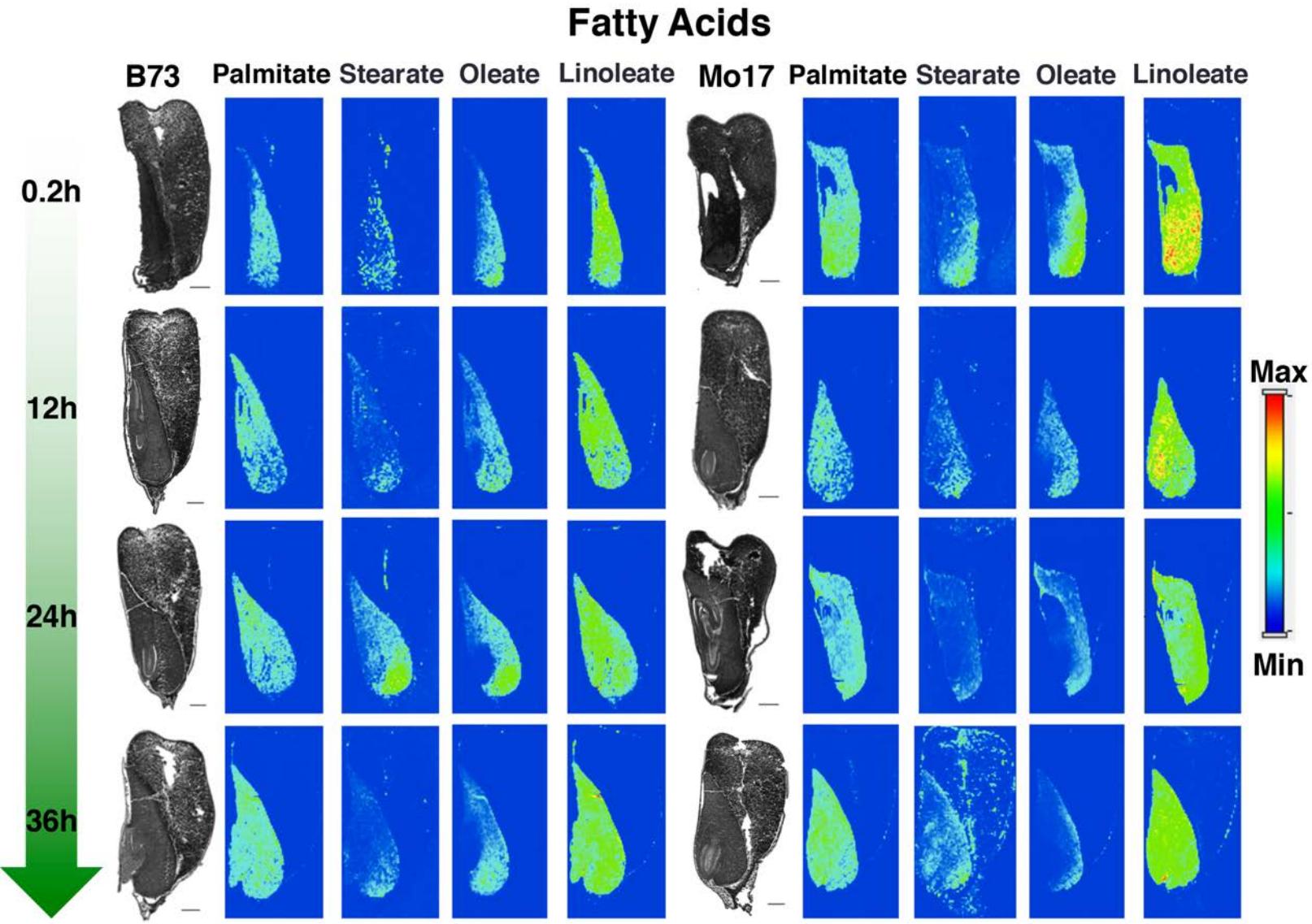

Fig. 6. Distribution of fatty acid species. All ions were detected as the deprotonated species, $[M-H]^-$, in negative ion mode with 9AA as the matrix. Scale bar: 1 mm. Stearate has some contamination from vacuum pump oil.

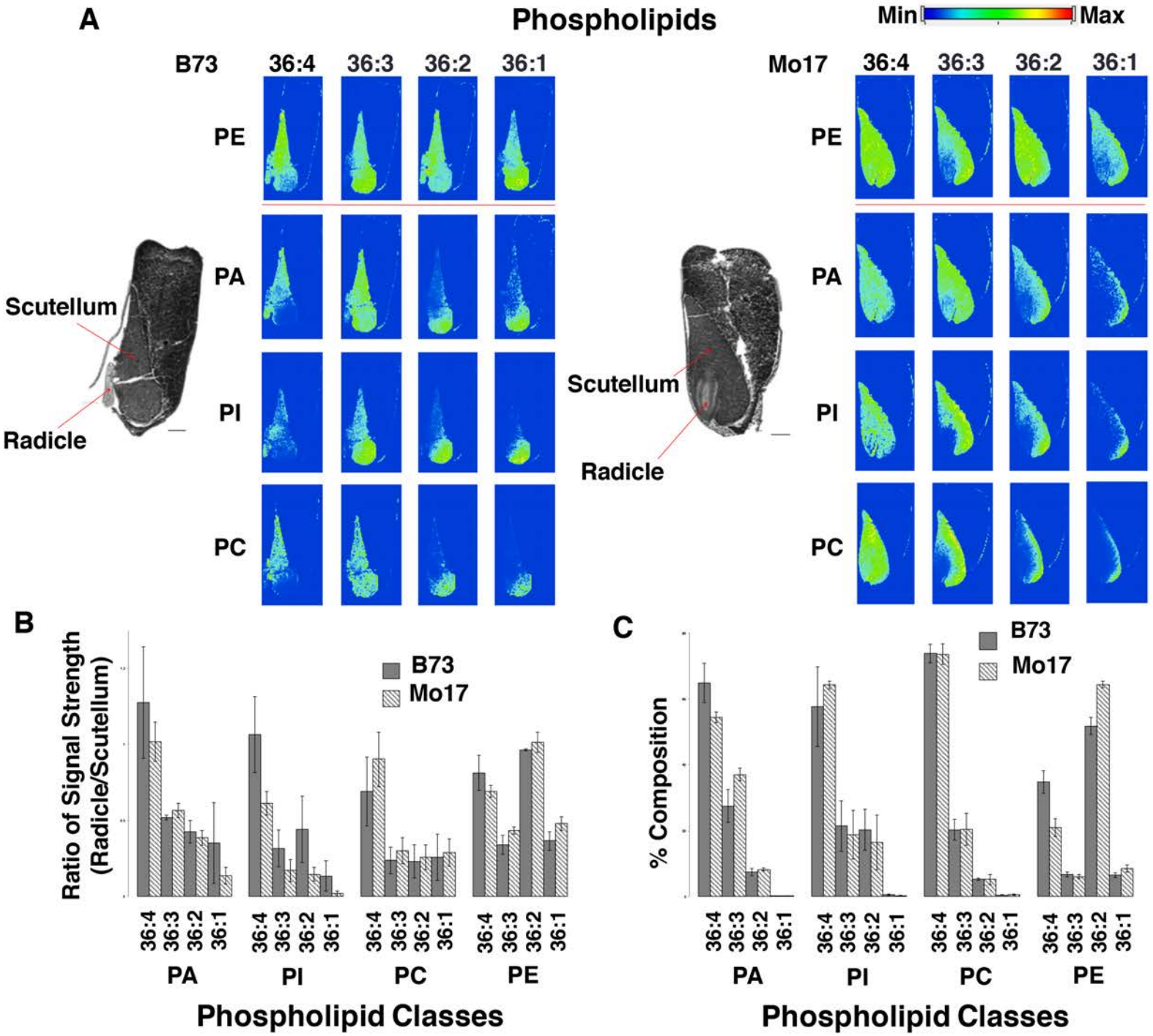

Fig. 7. Distribution and species analysis of various phospholipids. **(A)** Distribution of 16 different phospholipid molecular species in germinating seeds (36-h post imbibition). PE, PA, and PI are observed as deprotonated species, $[M-H]^-$, with DAN as the matrix in negative ion mode. PC is observed as a potassium adduct, $[M+K]^+$, with DHB matrix in positive ion mode. To allow direct comparisons, the optical images of the seeds were obtained from the adjacent cross-sections to those used to generate the MS images. Scale bar: 1 mm. Arrows in the radicle and scutellum regions of the embryo indicate the areas used to generate averaged mass spectra, from which semi-quantitative data of the phospholipids were gathered (see panels B and C). **(B)** Phospholipid ion signals in the radicle region normalized relative to the signals obtained from the scutellum. **(C)** Percentage of each molecular species within each phospholipid class in the radicle region.

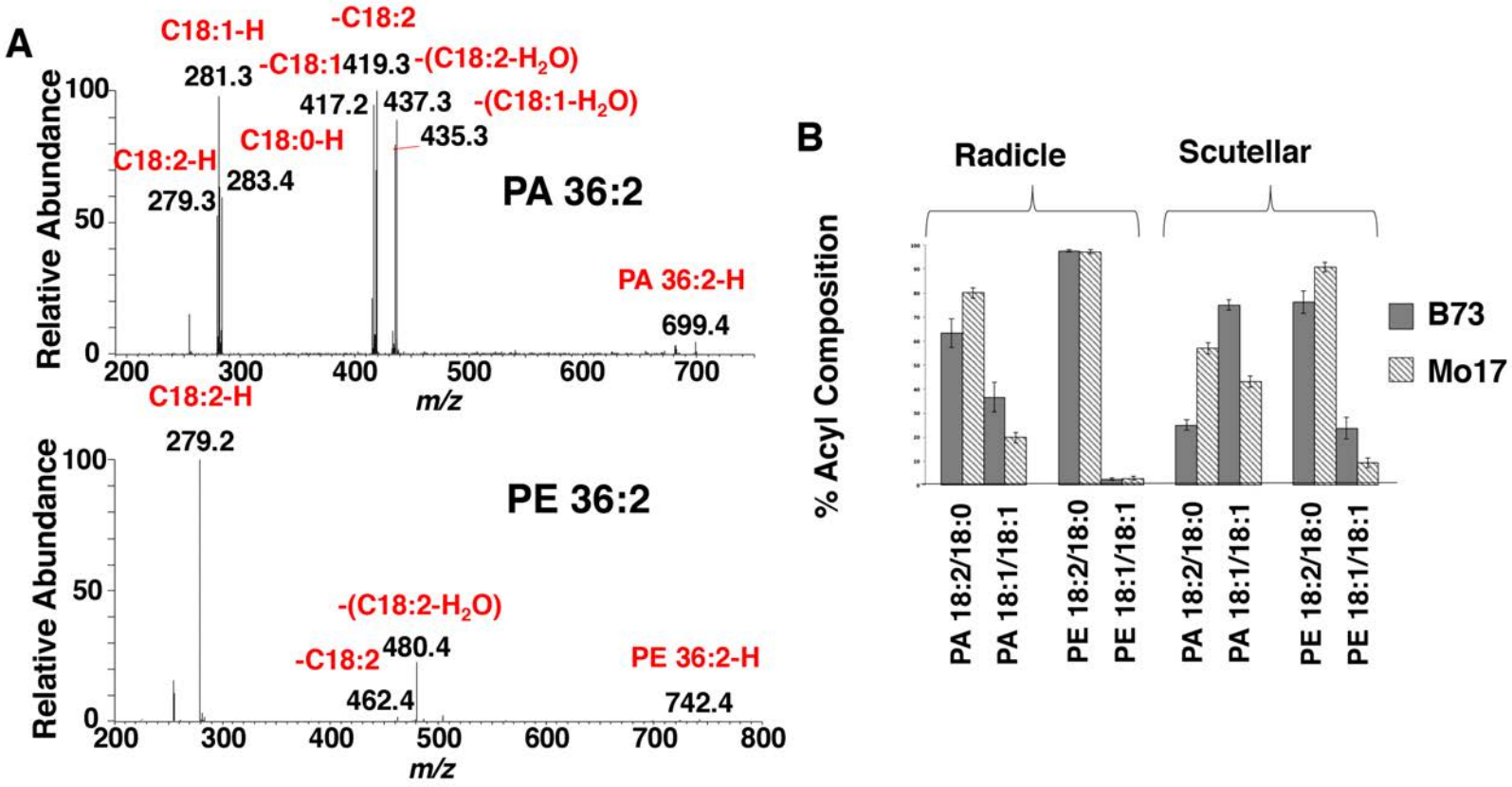

Fig. 8. MS/MS analysis of phospholipid species. **(A)** MS/MS spectra of PA 36:2 (top) and PE 36:2 (bottom) obtained from the radicle of a Mo17 inbred seed (24-hr post-imbibition). **(B)** Fatty acyl composition of different molecular species of PA 36:2 and PE 36:2, in the scutellum and radicle region of Mo17 and B73 seeds (24-hr post-imbibition).

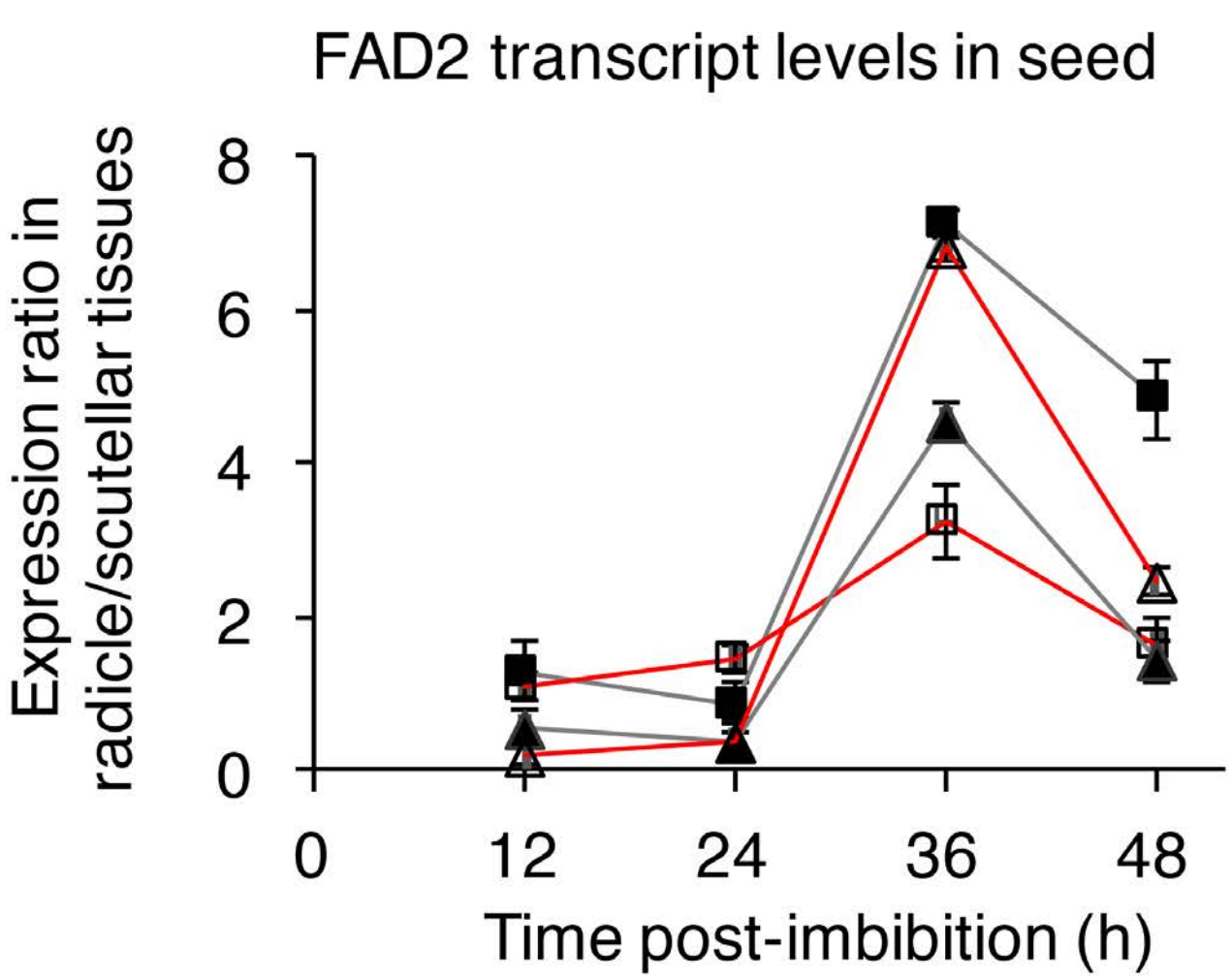

Fig. 9. Relative FAD2 expression in radicle and scutellar tissues of germinating maize seeds. FAD2 transcript levels encoded by GRMZM2G056252 (■, □) and GRMZM2G064701 (▲, △) were determined in RNA isolated from the radicle and scutellar tissues of germinating seeds from the inbreds B73 (—) and Mo17 (—)12-48-h post-imbibition. The expression of FAD2 transcripts was calculated by $2^{-(\Delta\Delta C_T)}$, using the ubiquitin mRNA (GenBank Accession Number: BT018032) as the internal control. Expression of each FAD2 transcript is normalized relative to the level found in the scutellar tissue.

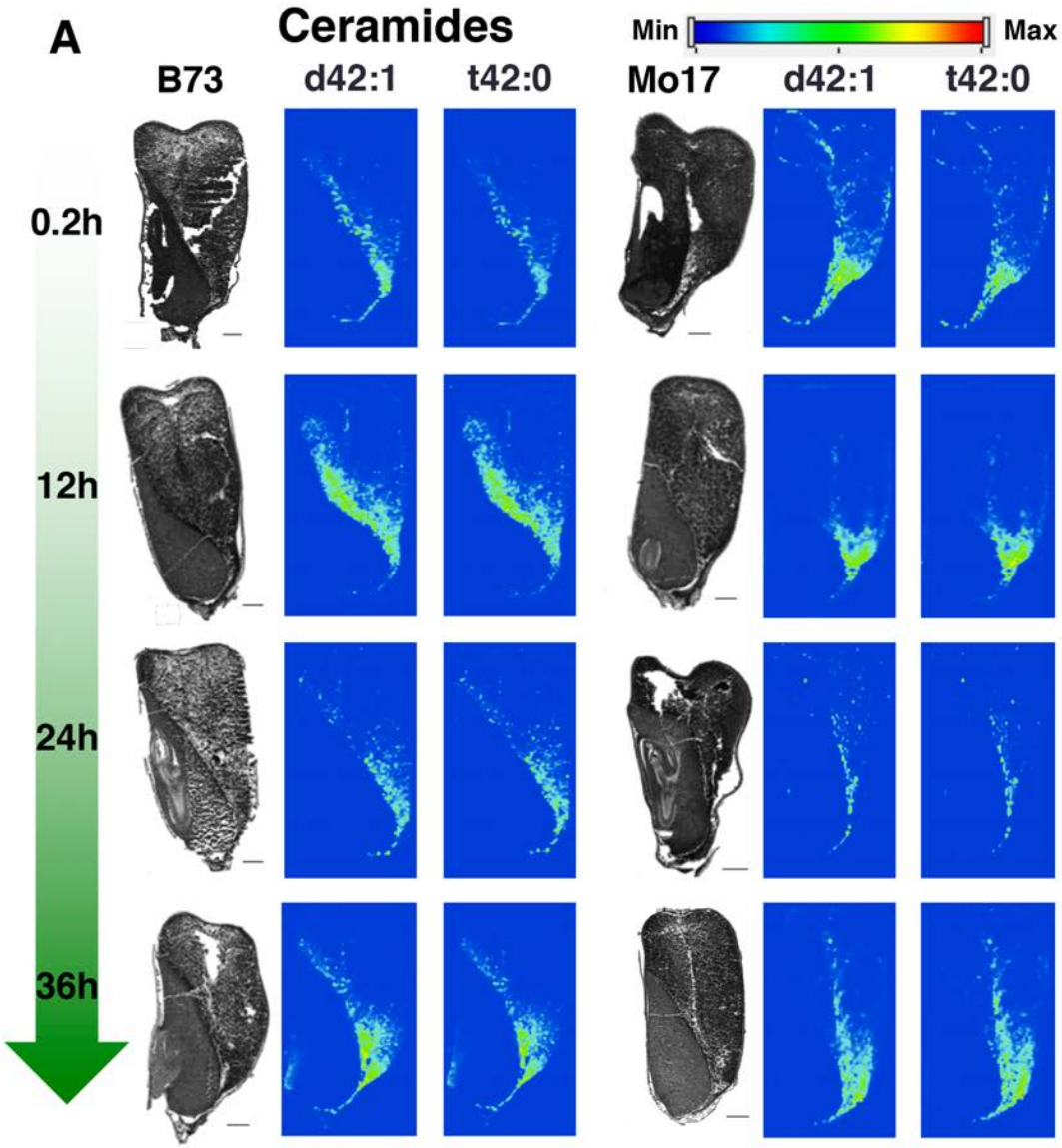

Fig. 10. Distribution of ceramide species. **(A)** Distributions of two ceramide molecular species (Cer d42:1, Cer t42:0). Both are detected as protonated species, $[M+H]^+$, in positive ion mode with DHB as the matrix. Scale bar: 1 mm. **(B)** Combined images of PC 34:2 (green) and ceramide d42:1 (red) in a B73 inbred seed at 12-h post-imbibition.

Parsed Citations

Anzala F, Morère-Le Paven M-C, Fournier S, Rondeau D, Limami AM (2006) Physiological and molecular aspects of aspartate-derived amino acid metabolism during germination and post-germination growth in two maize genotypes differing in germination efficiency. Journal of experimental botany 57: 645-653

Pubmed: Author and Title
CrossRef: Author and Title
Google Scholar: Author Only Title Only Author and Title

Bates PD, Stymne S, Ohlrogge J (2013) Biochemical pathways in seed oil synthesis. Current opinion in plant biology 16: 358-364

Pubmed: Author and Title
CrossRef: Author and Title
Google Scholar: Author Only Title Only Author and Title

Bernier AM, Ballance GM (1993) INDUCTION AND SECRETION OF ALPHA-AMYLASE, (1- 3),(1- 4)-BETA-GLUCANASE, AND (1- 3)-BETA-GLUCANASE ACTIVITIES IN GIBBERELLIC-ACID AND CACL2-TREATED HALF SEEDS AND ALEURONES OF WHEAT. Cereal Chemistry 70: 127-132

Pubmed: Author and Title
CrossRef: Author and Title
Google Scholar: Author Only Title Only Author and Title

Bewley JD (1997) Seed germination and dormancy. The plant cell 9: 1055

Pubmed: Author and Title
CrossRef: Author and Title
Google Scholar: Author Only Title Only Author and Title

Bewley JD (2001) Seed Germination and Reserve Mobilization. eLS

Pubmed: Author and Title
CrossRef: Author and Title
Google Scholar: Author Only Title Only Author and Title

Bewley JD, Bradford K, Hilhorst H (2012) Seeds: physiology of development, germination and dormancy. Springer Science & Business Media

Pubmed: Author and Title
CrossRef: Author and Title
Google Scholar: Author Only Title Only Author and Title

Chrispeels MJ, Varner J (1967) Hormonal control of enzyme synthesis: on the mode of action of gibberellic acid and abscisin in aleurone layers of barley. Plant physiology 42: 1008-1016

Pubmed: Author and Title
CrossRef: Author and Title
Google Scholar: Author Only Title Only Author and Title

Dante RA, Larkins BA, Sabelli PA (2015) Cell cycle control and seed development. Advances in Seed Biology: 21

Pubmed: Author and Title
CrossRef: Author and Title
Google Scholar: Author Only Title Only Author and Title

Dietrich CR, Perera M, D Yandeau-Nelson M, Meeley RB, Nikolau BJ, Schnable PS (2005) Characterization of two GL8 paralogs reveals that the 3-ketoacyl reductase component of fatty acid elongase is essential for maize (Zea mays L.) development. The Plant Journal 42: 844-861

Pubmed: Author and Title
CrossRef: Author and Title
Google Scholar: Author Only Title Only Author and Title

Feenstra AD, Hansen RL, Lee YJ (2015) Multi-matrix, dual polarity, tandem mass spectrometry imaging strategy applied to a germinated maize seed: toward mass spectrometry imaging of an untargeted metabolome. Analyst 140: 7293-7304

Pubmed: Author and Title
CrossRef: Author and Title
Google Scholar: Author Only Title Only Author and Title

Fincher GB (1989) Molecular and cellular biology associated with endosperm mobilization in germinating cereal grains. Annual review of plant biology 40: 305-346

Pubmed: Author and Title
CrossRef: Author and Title
Google Scholar: Author Only Title Only Author and Title

Firenzuoli A, Vanni P, Ramponi G, Baccari V (1968) Changes in enzyme levels during germination of seeds of Triticum durum. Plant physiology 43: 260-264

Pubmed: Author and Title
CrossRef: Author and Title
Google Scholar: Author Only Title Only Author and Title

Frank T, Scholz B, Peter S, Engel K-H (2011) Metabolite profiling of barley: Influence of the malting process. Food chemistry 124: 948-957

Pubmed: Author and Title
CrossRef: Author and Title
Google Scholar: Author Only Title Only Author and Title

Fu Y, Wen T-J, Ronin YI, Chen HD, Guo L, Mester DI, Yang Y, Lee M, Korol AB, Ashlock DA (2006) Genetic dissection of intermated

recombinant inbred lines using a new genetic map of maize. Genetics 174: 1671-1683
Pubmed: Author and Title
CrossRef: Author and Title
Google Scholar: Author Only Title Only Author and Title

Fujino Y, Ohnishi M, Ito S (1985) Molecular species of ceramide and mono-, di-, tri-, and tetraglycosylceramide in bran and endosperm of rice grains. Agricultural and biological chemistry 49: 2753-2762
Pubmed: Author and Title
CrossRef: Author and Title
Google Scholar: Author Only Title Only Author and Title

Guan X, Chen H, Abramson A, Man H, Wu J, Yu O, Nikolau BJ (2015) A phosphopantetheinyl transferase that is essential for mitochondrial fatty acid biosynthesis. The Plant Journal 84: 718-732
Pubmed: Author and Title
CrossRef: Author and Title
Google Scholar: Author Only Title Only Author and Title

Hankin JA, Barkley RM, Murphy RC (2007) Sublimation as a method of matrix application for mass spectrometric imaging. Journal of the American Society for Mass Spectrometry 18: 1646-1652
Pubmed: Author and Title
CrossRef: Author and Title
Google Scholar: Author Only Title Only Author and Title

He M, Zhu C, Dong K, Zhang T, Cheng Z, Li J, Yan Y (2015) Comparative proteome analysis of embryo and endosperm reveals central differential expression proteins involved in wheat seed germination. BMC plant biology 15: 1
Pubmed: Author and Title
CrossRef: Author and Title
Google Scholar: Author Only Title Only Author and Title

Hirsch CN, Foerster JM, Johnson JM, Sekhon RS, Muttoni G, Vaillancourt B, Peñagaricano F, Lindquist E, Pedraza MA, Barry K (2014) Insights into the maize pan-genome and pan-transcriptome. The Plant Cell 26: 121-135
Pubmed: Author and Title
CrossRef: Author and Title
Google Scholar: Author Only Title Only Author and Title

Horn PJ, Korte AR, Neogi PB, Love E, Fuchs J, Strupat K, Borisjuk L, Shulaev V, Lee Y-J, Chapman KD (2012) Spatial Mapping of Lipids at Cellular Resolution in Embryos of Cotton. The Plant Cell 24: 622-636
Pubmed: Author and Title
CrossRef: Author and Title
Google Scholar: Author Only Title Only Author and Title

Horn PJ, Silva JE, Anderson D, Fuchs J, Borisjuk L, Nazarenus TJ, Shulaev V, Cahoon EB, Chapman KD (2013) Imaging heterogeneity of membrane and storage lipids in transgenic Camelina sativa seeds with altered fatty acid profiles. Plant Journal 76: 138-150
Pubmed: Author and Title
CrossRef: Author and Title
Google Scholar: Author Only Title Only Author and Title

Hou W, Zhou H, Khalil MB, Seebun D, Bennett SA, Figeys D (2011) Lyso-form fragment ions facilitate the determination of stereospecificity of diacyl glycerophospholipids. Rapid Communications in Mass Spectrometry 25: 205-217
Pubmed: Author and Title
CrossRef: Author and Title
Google Scholar: Author Only Title Only Author and Title

Hu S, Lübberstedt T, Zhao G, Lee M (2016) QTL Mapping of Low-Temperature Germination Ability in the Maize IBM Syn4 RIL Population. PloS one 11: e0152795
Pubmed: Author and Title
CrossRef: Author and Title
Google Scholar: Author Only Title Only Author and Title

Hur M, Campbell AA, Almeida-de-Macedo M, Li L, Ransom N, Jose A, Crispin M, Nikolauh BJ, Wurtele ES (2013) A global approach to analysis and interpretation of metabolic data for plant natural product discovery. Natural Product Reports 30: 565-583
Pubmed: Author and Title
CrossRef: Author and Title
Google Scholar: Author Only Title Only Author and Title

Ingle J, Beevers L, Hageman R (1964) Metabolic changes associated with the germination of corn. I. Changes in weight and metabolites and their redistribution in the embryo axis, scutellum, and endosperm. Plant physiology 39: 735
Pubmed: Author and Title
CrossRef: Author and Title
Google Scholar: Author Only Title Only Author and Title

Kaspar S, Peukert M, Svatos A, Matros A, Mock HP (2011) MALDI-imaging mass spectrometry-An emerging technique in plant biology. Proteomics 11: 1840-1850
Pubmed: Author and Title
CrossRef: Author and Title
Google Scholar: Author Only Title Only Author and Title

Kolesnick R (2002) The therapeutic potential of modulating the ceramide/sphingomyelin pathway. The Journal of clinical investigation 110: 3-8

Pubmed: Author and Title
CrossRef: Author and Title
Google Scholar: Author Only Title Only Author and Title

Kollipara KP, Saab IN, Wych RD, Lauer MJ, Singletary GW (2002) Expression profiling of reciprocal maize hybrids divergent for cold germination and desiccation tolerance. Plant Physiology 129: 974-992
Pubmed: Author and Title
CrossRef: Author and Title
Google Scholar: Author Only Title Only Author and Title

Korte AR, Yandeau-Nelson MD, Nikolau BJ, Lee YJ (2015) Subcellular-level resolution MALDI-MS imaging of maize leaf metabolites by MALDI-linear ion trap-Orbitrap mass spectrometer. Analytical and bioanalytical chemistry 407: 2301-2309
Pubmed: Author and Title
CrossRef: Author and Title
Google Scholar: Author Only Title Only Author and Title

Lai J, Li R, Xu X, Jin W, Xu M, Zhao H, Xiang Z, Song W, Ying K, Zhang M (2010) Genome-wide patterns of genetic variation among elite maize inbred lines. Nature genetics 42: 1027-1030
Pubmed: Author and Title
CrossRef: Author and Title
Google Scholar: Author Only Title Only Author and Title

Larson G, Piperno DR, Allaby RG, Purugganan MD, Andersson L, Arroyo-Kalin M, Barton L, Vigueira CC, Denham T, Dobney K (2014) Current perspectives and the future of domestication studies. Proceedings of the National Academy of Sciences 111: 6139-6146
Pubmed: Author and Title
CrossRef: Author and Title
Google Scholar: Author Only Title Only Author and Title

Lee YJ, Perdian DC, Song Z, Yeung ES, Nikolau BJ (2012) Use of mass spectrometry for imaging metabolites in plants. Plant Journal 70: 81-95
Pubmed: Author and Title
CrossRef: Author and Title
Google Scholar: Author Only Title Only Author and Title

Leonova S, Grimberg Å, Marttila S, Stymne S, Carlsson AS (2010) Mobilization of lipid reserves during germination of oat (Avena sativa L.), a cereal rich in endosperm oil. Journal of experimental botany 61: 3089-3099
Pubmed: Author and Title
CrossRef: Author and Title
Google Scholar: Author Only Title Only Author and Title

Levy M, Futerman AH (2010) Mammalian ceramide synthases. IUBMB life 62: 347-356
Pubmed: Author and Title
CrossRef: Author and Title
Google Scholar: Author Only Title Only Author and Title

Limami AM, Rouillon C, Glevarec G, Gallais A, Hirel B (2002) Genetic and physiological analysis of germination efficiency in maize in relation to nitrogen metabolism reveals the importance of cytosolic glutamine synthetase. Plant Physiology 130: 1860-1870
Pubmed: Author and Title
CrossRef: Author and Title
Google Scholar: Author Only Title Only Author and Title

Liu W-Y, Chang Y-M, Chen SC-C, Lu C-H, Wu Y-H, Lu M-YJ, Chen D-R, Shih AC-C, Sheue C-R, Huang H-C (2013) Anatomical and transcriptional dynamics of maize embryonic leaves during seed germination. Proceedings of the National Academy of Sciences 110: 3979-3984
Pubmed: Author and Title
CrossRef: Author and Title
Google Scholar: Author Only Title Only Author and Title

Livak KJ, Schmittgen TD (2001) Analysis of Relative Gene Expression Data Using Real-Time Quantitative PCR and the 2-??CT Method. Methods 25: 402-408
Pubmed: Author and Title
CrossRef: Author and Title
Google Scholar: Author Only Title Only Author and Title

Lu H, Bernardo R (2001) Molecular marker diversity among current and historical maize inbreds. Theoretical and Applied Genetics 103: 613-617
Pubmed: Author and Title
CrossRef: Author and Title
Google Scholar: Author Only Title Only Author and Title

Luttgeharm KD, Chen M, Mehra A, Cahoon RE, Markham JE, Cahoon EB (2015) Overexpression of Arabidopsis ceramide synthases differentially affects growth, sphingolipid metabolism, programmed cell death, and mycotoxin resistance. Plant physiology 169: 1108-1117
Pubmed: Author and Title
CrossRef: Author and Title
Google Scholar: Author Only Title Only Author and Title

Lynch DV, Dunn TM (2004) An introduction to plant sphingolipids and a review of recent advances in understanding their metabolism and function. New phytologist 161: 677-702

Pubmed: Author and Title
CrossRef: Author and Title
Google Scholar: Author Only Title Only Author and Title

Markham JE, Lynch DV, Napier JA, Dunn TM, Cahoon EB (2013) Plant sphingolipids: function follows form. Current opinion in plant biology 16: 350-357
Pubmed: Author and Title
CrossRef: Author and Title
Google Scholar: Author Only Title Only Author and Title

McDonnell LA, Heeren R (2007) Imaging mass spectrometry. Mass spectrometry reviews 26: 606-643
Pubmed: Author and Title
CrossRef: Author and Title
Google Scholar: Author Only Title Only Author and Title

McDonnell LA, Heeren RMA (2007) Imaging mass spectrometry. Mass Spectrometry Reviews 26: 606-643
Pubmed: Author and Title
CrossRef: Author and Title
Google Scholar: Author Only Title Only Author and Title

Munamava MR, Goggi AS, Pollak L (2004) Seed quality of maize inbred lines with different composition and genetic backgrounds. Crop science 44: 542-548
Pubmed: Author and Title
CrossRef: Author and Title
Google Scholar: Author Only Title Only Author and Title

Nonogaki H (2008) Seed germination and reserve mobilization. eLS
Pubmed: Author and Title
CrossRef: Author and Title
Google Scholar: Author Only Title Only Author and Title

Petryszak R, Keays M, Tang YA, Fonseca NA, Barrera E, Burdett T, Füllgrabe A, Fuentes AM-P, Jupp S, Koskinen S, Mannion O, Huerta L, Megy K, Snow C, Williams E, Barzine M, Hastings E, Weisser H, Wright J, Jaiswal P, Huber W, Choudhary J, Parkinson HE, Brazma A (2016) Expression Atlas update—an integrated database of gene and protein expression in humans, animals and plants. Nucleic Acids Research 44: D746-D752
Pubmed: Author and Title
CrossRef: Author and Title
Google Scholar: Author Only Title Only Author and Title

Quanbeck SMM, Brachova L, Campbell AA, Guan X, Perera A, He K, Rhee SY, Bais P, Dickerson J, Dixon P (2012) Metabolomics as a hypothesis-generating functional genomics tool for the annotation of Arabidopsis thaliana genes of "unknown function". Frontiers in plant science 3: 15
Pubmed: Author and Title
CrossRef: Author and Title
Google Scholar: Author Only Title Only Author and Title

Römisch-Margl L, Spielbauer G, Schützenmeister A, Schwab W, Piepho H-P, Genschel U, Gierl A (2010) Heterotic patterns of sugar and amino acid components in developing maize kernels. Theoretical and Applied Genetics 120: 369-381
Pubmed: Author and Title
CrossRef: Author and Title
Google Scholar: Author Only Title Only Author and Title

Samuels KMS, Wada H, Welti R, Xu C, Zallot R, Ohlrogge J (2013) Acyl-lipid metabolism. The Arabidopsis Book 1: 70
Pubmed: Author and Title
CrossRef: Author and Title
Google Scholar: Author Only Title Only Author and Title

Sánchez-Linares L, Gavilanes-Ruíz M, Díaz-Pontones D, Guzmán-Chávez F, Calzada-Alejo V, Zurita-Villegas V, Luna-Loaiza V, Moreno-Sánchez R, Bernal-Lugo I, Sánchez-Nieto S (2012) Early carbon mobilization and radicle protrusion in maize germination. Journal of experimental botany: ers130
Pubmed: Author and Title
CrossRef: Author and Title
Google Scholar: Author Only Title Only Author and Title

Schmidt MA, Barbazuk WB, Sandford M, May G, Song Z, Zhou W, Nikolau BJ, Herman EM (2011) Silencing of soybean seed storage proteins results in a rebalanced protein composition preserving seed protein content without major collateral changes in the metabolome and transcriptome. Plant Physiology 156: 330-345
Pubmed: Author and Title
CrossRef: Author and Title
Google Scholar: Author Only Title Only Author and Title

Schnable PS, Ware D, Fulton RS, Stein JC, Wei F, Pasternak S, Liang C, Zhang J, Fulton L, Graves TA (2009) The B73 maize genome: complexity, diversity, and dynamics. science 326: 1112-1115
Pubmed: Author and Title
CrossRef: Author and Title
Google Scholar: Author Only Title Only Author and Title

Sen TZ, Harper LC, Schaeffer ML, Andorf CM, Seigfried TE, Campbell DA, Lawrence CJ (2010) Choosing a genome browser for a Model Organism Database: surveying the Maize community. Database-the Journal of Biological Databases and Curation
Pubmed: Author and Title
CrossRef: Author and Title

Google Scholar: Author Only Title Only Author and Title

Shu X-L, Frank T, Shu Q-Y, Engel K-H (2008) Metabolite profiling of germinating rice seeds. Journal of agricultural and food chemistry 56: 11612-11620
Pubmed: Author and Title
CrossRef: Author and Title
Google Scholar: Author Only Title Only Author and Title

Springer NM, Ying K, Fu Y, Ji T, Yeh C-T, Jia Y, Wu W, Richmond T, Kitzman J, Rosenbaum H (2009) Maize inbreds exhibit high levels of copy number variation (CNV) and presence/absence variation (PAV) in genome content. PLoS Genet 5: e1000734
Pubmed: Author and Title
CrossRef: Author and Title
Google Scholar: Author Only Title Only Author and Title

Stein SE (1999) An integrated method for spectrum extraction and compound identification from gas chromatography/mass spectrometry data. Journal of the American Society for Mass Spectrometry 10: 770-781
Pubmed: Author and Title
CrossRef: Author and Title
Google Scholar: Author Only Title Only Author and Title

Swanson-Wagner RA, Eichten SR, Kumari S, Tiffin P, Stein JC, Ware D, Springer NM (2010) Pervasive gene content variation and copy number variation in maize and its undomesticated progenitor. Genome research 20: 1689-1699
Pubmed: Author and Title
CrossRef: Author and Title
Google Scholar: Author Only Title Only Author and Title

Toue S, Sugiura Y, Kubo A, Ohmura M, Karakawa S, Mizukoshi T, Yoneda J, Miyano H, Noguchi Y, Kobayashi T (2014) Microscopic imaging mass spectrometry assisted by on-tissue chemical derivatization for visualizing multiple amino acids in human colon cancer xenografts. Proteomics 14: 810-819
Pubmed: Author and Title
CrossRef: Author and Title
Google Scholar: Author Only Title Only Author and Title

Troyer AF (2004) Persistent and popular germplasm in seventy centuries of corn evolution. Corn: Origin, History, and Production. John Wiley & Sons, Hoboken, NJ: 133-231
Pubmed: Author and Title
CrossRef: Author and Title
Google Scholar: Author Only Title Only Author and Title

Troyer AF (2009) Development of hybrid corn and the seed corn industry. In Handbook of maize. Springer, pp 87-114
Pubmed: Author and Title
CrossRef: Author and Title
Google Scholar: Author Only Title Only Author and Title

van Hove ERA, Smith DF, Heeren RM (2010) A concise review of mass spectrometry imaging. Journal of Chromatography A 1217: 3946-3954
Pubmed: Author and Title
CrossRef: Author and Title
Google Scholar: Author Only Title Only Author and Title

Vroh Bi I, McMullen M, Sanchez-Villeda H, Schroeder S, Gardiner J, Polacco M, Soderlund C, Wing R, Fang Z, Coe E (2006) Single nucleotide polymorphisms and insertion-deletions for genetic markers and anchoring the maize fingerprint contig physical map. Crop science 46: 12-21
Pubmed: Author and Title
CrossRef: Author and Title
Google Scholar: Author Only Title Only Author and Title

Wang G, Wang G, Zhang X, Wang F, Song R (2012) Isolation of High Quality RNA from Cereal Seeds Containing High Levels of Starch. Phytochemical Analysis 23: 159-163
Pubmed: Author and Title
CrossRef: Author and Title
Google Scholar: Author Only Title Only Author and Title

Williams LD, Glenn AE, Zimeri AM, Bacon CW, Smith MA, Riley RT (2007) Fumonisin disruption of ceramide biosynthesis in maize roots and the effects on plant development and Fusarium verticillioides-induced seedling disease. Journal of agricultural and food chemistry 55: 2937-2946
Pubmed: Author and Title
CrossRef: Author and Title
Google Scholar: Author Only Title Only Author and Title

Ye J, Coulouris G, Zaretskaya I, Cutcutache I, Rozen S, Madden TL (2012) Primer-BLAST: A tool to design target-specific primers for polymerase chain reaction. BMC Bioinformatics 13: 134
Pubmed: Author and Title
CrossRef: Author and Title
Google Scholar: Author Only Title Only Author and Title

Zavalin A, Yang J, Caprioli R (2013) Laser Beam Filtration for High Spatial Resolution MALDI Imaging Mass Spectrometry. Journal of The American Society for Mass Spectrometry 24: 1153-1156
Pubmed: Author and Title
CrossRef: Author and Title

Google Scholar: Author Only Title Only Author and Title

Zeeman SC, Delatte T, Messerli G, Umhang M, Stettler M, Mettler T, Streb S, Reinhold H, Kötting O (2007) Starch breakdown: recent discoveries suggest distinct pathways and novel mechanisms. In, Vol 34. CSIRO Publishing, Functional Plant Biology, pp 465-473

Pubmed: Author and Title
CrossRef: Author and Title
Google Scholar: Author Only Title Only Author and Title

Zhang M, Fan J, Taylor DC, Ohlrogge JB (2009) DGAT1 and PDAT1 acyltransferases have overlapping functions in Arabidopsis triacylglycerol biosynthesis and are essential for normal pollen and seed development. The Plant Cell 21: 3885-3901

Pubmed: Author and Title
CrossRef: Author and Title
Google Scholar: Author Only Title Only Author and Title